

REVIEW

View Article Online

View Journal | View Issue



Cite this: *Inorg. Chem. Front.*, 2018, **5**, 279

Liquid-free single-crystal to single-crystal transformations in coordination polymers

Wen-Wen He,^a Shun-Li Li^{*b} and Ya-Qian Lan ^{*b}

The design and synthesis of functional materials with desired properties is the ultimate goal for chemical pursuers. Single-crystal to single-crystal (SCSC) transformations are an important component of solid-state reactions. These transformations not only create new materials but also provide an opportunity to explore the process of forming a chemical bond, which is conducive to making function-oriented crystal synthesis a reality. In this review, we provide a broad overview of SCSC transformations that take place in polymers or metal-organic frameworks, and classify them into several groups based on their various inducing stimuli, such as UV light, loss/uptake of solvent vapor, temperature change, mechanical force and their synergic impact. Unlike other reviews, the SCSC transformations discussed in this paper are confined to transformations *via* an absolutely liquid-free mode (both the reactant and product are in the solid phase), while those involving liquids, in which the transformation occurs in a recrystallization manner, are strictly excluded. These dynamic processes all involve the breakage and formation of covalent or non-covalent bonds, accompanied by drastic structural rearrangement in the crystalline phase. Changes in the physical properties of these complexes resulting from SCSC transformations are also illustrated. Thanks to the regular characteristics of crystal structures before and after the reactions, the transformation processes may provide deep insights into the rational design of crystalline materials.

Received 18th November 2017,
Accepted 20th December 2017

DOI: 10.1039/c7qi00724h

rsc.li/frontiers-inorganic

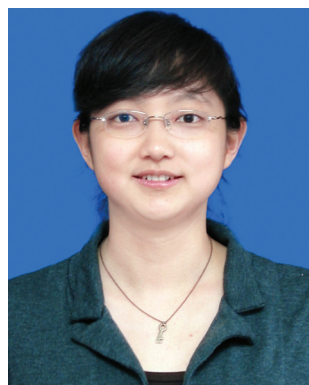
^aSchool of Chemistry and Life Science, Advanced Institute of Materials Science, Changchun University of Technology, Changchun 130012, China.

E-mail: heww@ccut.edu.cn

^bJiangsu Key Laboratory of Biofunctional Materials, School of Chemistry and Materials Science, Nanjing Normal University, Nanjing, 210023, Jiangsu, P. R. China. E-mail: yqlan@njnu.edu.cn, slli@njnu.edu.cn

1. Introduction

With increasing applications in the fields of energy, catalysis and bio-applications, functional inorganic-organic hybrid materials have become a major focus at the forefront of



Wen-Wen He

Wen-Wen He was born in 1987 in Jilin, P. R. China. She received her B.S. (2011) and Ph.D. degree (2016) from Faculty of Chemistry, Northeast Normal University (NENU) under the supervision of Prof. Zhong-Min Su and Prof. Ya-Qian Lan. Since the autumn of 2016, she has been a Lecturer of Chemistry at Changchun University of Technology (CCUT). Her current research interests focus on the development of POM-based

materials and MOF materials for applications in catalysis, separation and energy storage.



Shun-Li Li

Shun-Li Li was born in 1979 in Jilin, P. R. China. She received her B.S. (2002) in Chemistry and Ph.D. degree (2008) from Northeast Normal University under the supervision of Prof. Jian-Fang Ma. She carried out postdoctoral studies with Prof. Zhong-Min Su in Environmental Chemistry at NENU. Then she worked as a JSPS (Japan Society for the Promotion of Science) invited fellow at AIST (National Institute of Advanced Industrial

Science and Technology) in 2012. She is now a Professor of Chemistry at Nanjing Normal University. Her current research interest lies in the syntheses, structures and properties of polyoxo-metalate-based materials.

materials science.^{1–8} The synthesis of functional materials with desired properties and achieving control over molecular arrangement are the ultimate goals of chemical pursuers, which require an improved understanding of the formation process of chemical bonds.^{9–13} Reactions in the solid state provide a direct and effective method to investigate the nature of chemical reactions, since there is usually only one variable factor, free from solvents and other factors.^{14,15} Compared with bulk reactions in the other two phases, reactions in the solid state involve an entirely different process, and can be regulated to a much higher degree. In liquid or gas, molecules possess much freedom in their movements. In comparison, reactants in the solid phase have a more confined arrangement, owing to the effect of close molecular packing. Because of this restricted migration and non-aligning orientation of reactive functional groups, reactions in the solid state are relatively sluggish in general. It is this slow process of change that provides a more convenient method for us to study the cleavage and formation of chemical bonds. This especially occurs in crystalline state materials, in which molecules are rigidly and steadily fixed within crystal lattices.^{16,17}

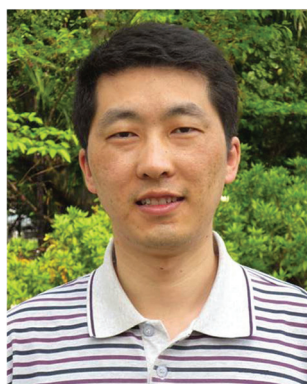
In the 1960s, the classical work of Gerhard Schmidt established the field of crystal engineering with the help of solid-state organic photochemistry.¹⁸ He showed that reactions can be easily facilitated in the solid state when the reactive functional groups are close and in the correct orientation. Nowadays, with developments in crystal engineering, single-crystal to single-crystal (SCSC) transformations have become an important component of solid-state reactions.¹⁹ Specific structural information of the reactants and the products in SCSC transformations can be obtained from X-ray diffraction analysis directly. Thanks to the regular characteristics of crystal structures, researchers can study the transformation process and mechanism more visually and intuitively. Thus, SCSC transformations not only produce target complexes that may be impossible to obtain *via* solvent reactions or modify as-synthesized materials with distinctive physicochemical prop-

erties, but can also provide an opportunity to explore the essence of these solid-state reactions. Studying the process of new bond formation in the crystalline state is the only way to make function-oriented crystal synthesis into a reality.

Single-crystal X-ray diffraction analysis is the most powerful method to obtain the detailed structure of a complex before and after a structural transformation has taken place.^{20,21} Preservation of the single-crystalline nature is the prerequisite for this analytical method. Although modern instruments mean that a single crystal suitable for X-ray diffraction analysis is much less restricted by its size and quality than before, sometimes the crystal after a solid-state structural transformation is too small or of inferior quality for single-crystal X-ray crystallography determinations. In these situations, techniques for determining structures from powder X-ray diffraction patterns have become a useful assistant. Other spectroscopic and analytical tools, such as nuclear magnetic resonance (NMR), X-ray photoelectron spectroscopy (XPS), scanning electron microscopy (SEM) and special methods including energy dispersive X-ray spectroscopy (EDX) and atomic force microscopy (AFM), have also been used to further study these solid-state reactions. Thanks to developments in instrument capabilities that facilitate the rapid collection of data, greater detail on dynamic structural transformations can now be obtained.

There have been a few reviews referring to SCSC transformations over the past few years, covering the vast area of the dynamic behaviors of coordination polymers.^{22,23} Among them, Vittal,^{24a} Chen^{24b,c} and Du²⁵ have contributed a lot. However, there is no review focused on the development of SCSC transformations in only the liquid-free solid state. Unlike other reviews, the SCSC transformations discussed in this paper are confined to transformations in an absolutely liquid-free mode (both the reactant and product are in solid phase), and those involving liquids, in which the transformation occurs in a recrystallization manner, are strictly excluded. These dynamic processes must involve the breakage and formation of covalent or non-covalent bonds, accompanied by drastic structural rearrangement in the crystalline phase. In addition, with regards to SCSC reactions, there is an emphasis on crystallinity with no disintegration. In some cases, a change of the whole crystal structure results in the breaking of crystals to some extent, but research has shown that these small chips often still maintain their crystallinity, and so these transformations are also within the scope of this paper. Examples discussed in this paper all involve crystalline materials, including coordination polymers (CPs), coordination supramolecular systems (CSSs), metal–organic frameworks (MOFs) and metal organic materials (MOMs). Only subtle differences exist amongst these terms, so they are not treated separately in this review.

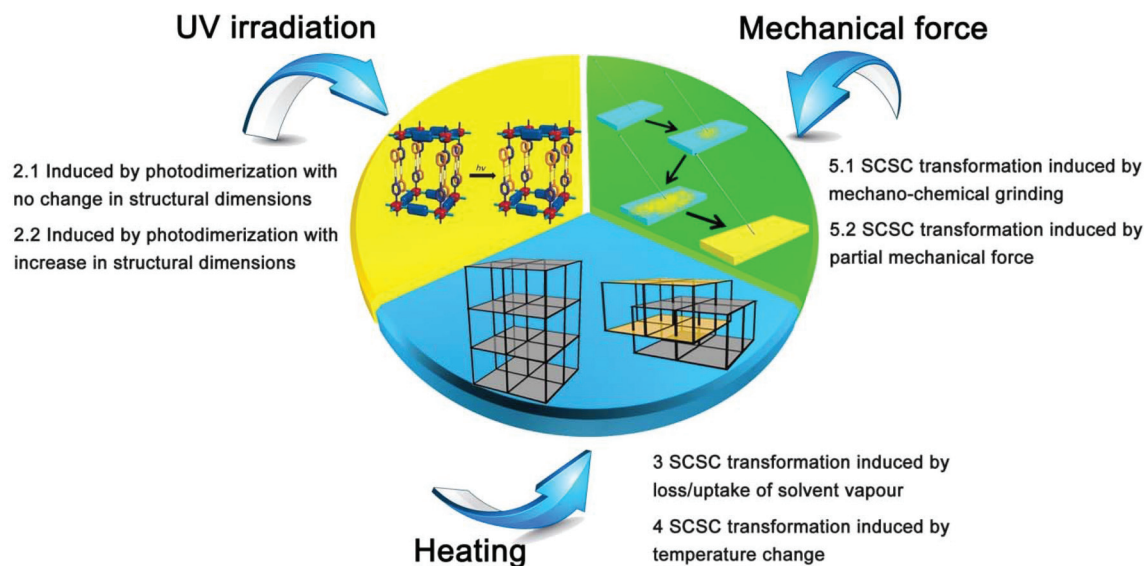
In this review, we will investigate recent examples of SCSC transformations in the literature and classify these phenomena in terms of different exogenous stimuli (Scheme 1), including UV light, loss/uptake of solvent vapor, temperature change, mechanical force and synergic effects. Structural transformations of this kind are often manifested by the



Ya-Qian Lan

Ya-Qian Lan was born in 1978 in Jilin, P. R. China. He received his B.S. and Ph.D. degree (2009) from Faculty of Chemistry, Northeast Normal University under the supervision of Prof. Zhong-Min Su. In 2010, he worked as a JSPS postdoctoral fellow at AIST. Since the fall of 2012, he has been a Professor of Chemistry at Nanjing Normal University. His current research interests focus on the application of polyoxometalate-based com-

posite materials in energy storage and conversion and porous metal–organic frameworks for applications in catalysis.



Scheme 1 Schematic of the classification of SCSC transformations discussed in this review.

changes taking place in building units (coordination number, geometry of the metal and component of the ligands), dimensionality and entanglement characteristics of the frameworks, *etc.* We will explore 57 complexes in total and number them in sequence. Structures before transformations will be named **X**, and the transformed structures will be named **X'** (or **X''**). Changes in the physical properties of the complexes resulting from SCSC transformations, such as the crystal color, magnetism, porosity, conductivity, luminescence, optics, chirality, catalysis and optics, will also be discussed.

2. SCSC transformation in the form of [2 + 2] photochemical reactions

Reactions induced by UV irradiation have fascinated many chemists over the past decade, as they provide an unmatched approach to achieve molecular rearrangement or transformation without the need for other environmental conditions (Table 1). Topochemical reactions and SCSC transformations have been extensively studied in organic chemistry.^{26–28} Compared to solid-state photochemical reactions involving two molecules, transformations of one coordination polymeric structure into another are relatively rarely reported in solid-state supramolecular reactions, as the breaking and forming of bonds should occur in more than one direction simultaneously.²⁹ This emerging field offers a potential way to synthesize new materials that cannot be obtained by traditional synthetic routes. 1,2-Bis(4'-pyridyl)ethylene, popularly known as bpe, has been widely used to design photoreactive coordination polymers, and in recent years, other asymmetric ligands that contain alkenyl groups have also been gradually explored (Scheme 2). In this section, we will separate these structural transformations into two parts according to whether

the dimension of the whole structure changes. In each part, we will discuss these complexes with the law of dimension from low to high.

2.1 SCSC transformation induced by photodimerization with no change in structural dimensions

Early in 2005, Vittal's group successfully synthesized a 1D complex $[(F_3CCO_2)(\mu-O_2CCH_3)Zn]_2(\mu-bpe)_2)_n$ (**1**) with the bpe ligand, which could undergo a 1D to 1D SCSC structural transition after being subjected to UV irradiation.²⁹ X-ray crystallography analysis showed that Zn(II) ions in **1** are bridged by two acetato ligands to form a molecular ladder polymer. UV irradiation of single crystals of **1** for about 3 h gave another single crystal $[(F_3CCO_2)(\mu-O_2CCH_3)Zn]_2(\mu-tpcb)_2)_n$ (**1'**) as shown in Fig. 1. During this transition, there was no change in its single-crystal nature, morphology or transparency. Single-crystal X-ray diffraction analysis confirmed the formation of new bonds and showed that the two pyridyl rings in **1'** are bent towards each other with an interplanar angle of 27.4°. In order to complete this transformation, the Zn...Zn distance increased and other bond parameters in **1** also changed to accommodate the formation of new single bonds. The formation of tpcb from two bpe ligands in the bulk of **1'** was also confirmed by ¹H NMR spectroscopy.

In 2011, another 1D to 1D photo-polymerization based on bpe ligands was reported by Lang's group.³⁰ In complex $[Cd(bpe)(CBA)_2]_n$ (**2**, HCBA = 4-chlorobenzoic acid), each pair of Cd atoms is linked by four CBA ligands to form a $[Cd_2(\eta-\mu-CBA)_2(\eta,\eta-CBA)_2]$ unit. This unit connects to its neighboring ones *via* a pair of bpe bridges to form a 1D $[Cd_2(bpe)_2(CBA)_4]_n$ double-chain. Each pair of bpe ligands in **2** is arranged parallelly, and the C...C distance between two adjacent bpe ligands is 3.771 Å. This geometry conforms to Schmidt's topochemical criteria for photochemical [2 + 2] cycloaddition. Under UV

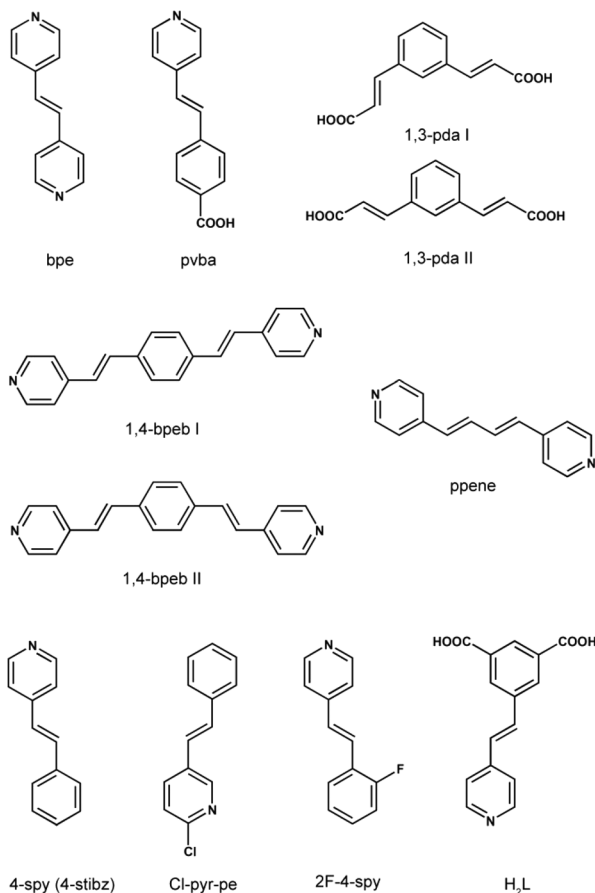
Table 1 Single-crystal to single-crystal transformations triggered by UV Irradiation

No.	Compounds before SCSC	CCDC refcode	Compounds after SCSC	CCDC refcode	Ligands before SCSC	Ligands after SCSC	Dimensionality	Irradiation source	Time	Ref.
1	$[(\text{Fe}_3\text{CCO}_2)(\mu\text{-O}_2\text{CCH}_3)_2\text{Zn}]_2(\mu\text{-bpe})_2$	255236	$[(\text{Fe}_3\text{CCO}_2)(\mu\text{-O}_2\text{CCH}_3)_2\text{Zn}]_2(\mu\text{-tpcb})_2$	255237	$\mu\text{-bpe}$	$\mu\text{-tpcb}$ tpcb = tetrakis(4-pyridyl)-cyclobutane	1D \rightarrow 1D	UV irradiation	3 h	29
2	$[\text{Cd}(\text{bpe})(\text{CBA})_2]$	772183	$[\text{Cd}(\text{rtt-tpcb})_{0.5}(\text{CBA})_2]$	772184	bpe	rtt-tpcb rtt-tpcb = rtt-tetrakis(4-pyridyl)cyclobutane	1D \rightarrow 1D	UV irradiation	5 h	30
3	$[\text{Cd}_2(\text{pvba})_2(\text{tbdc})(\text{dmf})_2]$	856465	— ^a	— ^b	pvba	bcbpcb bcbpcb = rtt-1,3-bis(4'-carboxyphenyl)-2,4-bis(4"-pyridyl)cyclobutane	2D \rightarrow 2D	UV light	15 min	31
4	$[\text{Co}_2(\text{pvba})_2(\text{tbdc})(\text{dmf})_2(\text{H}_2\text{O})_2]$	856466	— ^a	— ^b	pvba	bcbpcb	2D \rightarrow 2D	UV light	4 h	31
5	$[\text{Ni}_2(\text{pvba})_2(\text{tbdc})(\text{dmf})_2(\text{H}_2\text{O})_2]$	— ^c	— ^a	— ^b	pvba	bcbpcb	2D \rightarrow 2D	UV light	4 h	31
6	$[\text{Mn}(\text{1,4-bpeb})(\text{1,3-pda})](\text{1,4-bpeb})_n$	953920	— ^a	— ^b	1,4-bpeb	tpcp	2D \rightarrow 2D	UV light with different wavelength	Different times	32
7	$[\text{Zn}(\text{bpe})(\text{muco})]\cdot\text{DMF}\cdot\text{H}_2\text{O}$	751094	$[\text{Zn}(\text{rtt-tpcb})_{1/2}(\text{muco})]\cdot\text{DMF}\cdot\text{H}_2\text{O}$	751097	bpe	tpcp tpcp = tetrakis(4-pyridyl)-1,2,9,10-diethano[2.2]paracyclophane	3D \rightarrow 3D	Xenon light	30 min	33
8	$[\text{Zn}(\text{bpe})(\text{bdc})]\cdot\text{DMF}$	751095	$[\text{Zn}(\text{rtt-tpcb})_{1/2}(\text{bdc})]\cdot\text{DMF}$	751098	bpe	rtt-tpcb	3D \rightarrow 3D	Xenon light	30 min	33
9	$[\text{Zn}(\text{bpe})(\text{fum})]$	751096	— ^a	— ^b	bpe	rtt-tpcb	3D \rightarrow 3D	Xenon light	30 min	33
10	$[\text{Zn}_4(\text{t}_3\text{-OH})_2(5\text{-sipa})_2(1,4\text{-bpeb})_2]\cdot 4\text{H}_2\text{O}$	761121	$[\text{Zn}_4(\text{t}_3\text{-OH})_2(5\text{-sipa})_2(\text{bpbvpccb})]\cdot 2\text{H}_2\text{O}$	761122	1,4-bpeb	bpbvpccb bpbvpccb = 1,3-bis(4-pyridyl)-2,4-bis[4-(2-(4-pyridyl)-vinyl)phenyl]cyclobutane	3D \rightarrow 3D	Hg lamp (400 W)	8 h	34
11	$\{\text{Cd}_2(1,3\text{-pda})_2(1,4\text{-bpeb})_2\}_n$	761123	$\{\text{Cd}_2(1,3\text{-pda})_2(\text{tpcp})\}_n$	761124	1,4-bpeb	tpcp	3D \rightarrow 3D	Hg lamp (400 W)	10 h	34
12	$[\text{Zn}_2(\text{bpeb})(\text{bdc})(\text{fa})_2]$	955835	$[\text{Zn}_2(\text{poly-bppcb})(\text{bdc})(\text{fa})_2]\cdot\text{H}_2\text{O}$	955836	bpeb	poly-bppcb poly-bppcb = 1,3-(4,4'-bipyridyl)-2,4-phenylene-cyclobutane	3D \rightarrow 3D	Xe-lamp of wavelength 365 nm	2 h	35
13	$[\text{Cd}(\text{ppene})(1,4\text{-BDC})]\cdot\text{MeCN}$	1038884	$[\{\text{Cd}_2(4\text{-tp-3-lad})(1,4\text{-BDC})_2\}\cdot 2\text{MeCN}]_n$	1518019	ppene	4-tp-3-lad 4-tp-3-lad = 2,3,5,6-tetra(pyridin-4-yl)-bicyclo[2.2.0]hexane	3D \rightarrow 3D	400 W high-pressure Hg-lamp 365 nm	12 h	36
14	$[\text{Ag}_2(4\text{-stilbz})_4][\text{CO}_3\text{CF}_3]_2$	261658	$[\text{Ag}_2(4\text{-pyr-ph-cb})_2][(\text{CO}_3\text{CF}_3)_2]$	261660	4-stilbz	4-pyr-ph-cb 4-pyr-ph-cb = rtt-1,2-bis(4-pyridyl)-3,4-bis(phenyl)cyclobutane	0D \rightarrow 1D	500 W Hg lamp	18 h	37
15	$\text{Ag}_2(\text{Cl-pyr-pe})_4[\text{ClO}_3]_2$	898413	$\text{Ag}_2(\text{Cl-pyr-pe})_2(\text{Cl-pyr-p-cb})[\text{ClO}_3]_2$	898414	Cl-pyr-pe	Cl-pyr-p-cb Cl-pyr-p-cb = rett-1,3-bis(4-Cl-3-pyridyl)-2,4-bis(phenyl)-cyclobutane	0D \rightarrow 1D	broadband 450 W medium-pressure Hg-lamp	48 h	38
16	$[\text{Ag}_2(4\text{-stilbz})_4][\text{CF}_3\text{SO}_3]_2$	945407	$[\text{Ag}_2(4\text{-pyr-ph-cb})_2][\text{CF}_3\text{SO}_3]_2$	945408	4-stilbz	4-pyr-ph-cb	0D \rightarrow 0D	broadband UV irradiation	30 h	39

Table 1 (Contd.)

No.	Compounds before SCSC	CCDC refcode	Compounds after SCSC	CCDC refcode	Ligands before SCSC	Ligands after SCSC	Dimensionality	Irradiation source	Time	Ref.
17	$[\text{ZnBr}_2(4\text{-spy})_2]$	938967	$[\text{ZnBr}_2(\text{rtt}-\text{ppcb})]$	938968	4-spy	<i>rtt</i> -ppcb <i>rtt</i> -ppcb = <i>rtt</i> -1,3-bis(4'-pyridyl)-2,4-bis(phenyl)cyclobutane	0D → 1D	UV irradiation	60 h	40
18	$[\text{ZnBr}_2(2\text{F-4spy})_2]$	938969	$[\text{ZnBr}_2(\text{rtt}-\text{F-ppcb})]$	938970	2F-4spy	<i>rtt</i> -F-ppcb <i>rtt</i> -F-ppcb = <i>rtt</i> -1,3-bis(4'-pyridyl)-2,4-bis(2'-fluoro-phenyl)cyclobutane	0D → 1D	UV irradiation	36 h	40
19	$[\text{Pb}_3(\mu\text{-bpe})_3(\mu\text{-O}_2\text{CCH}_3)_2(\mu\text{-O}_2\text{CCF}_3)_4(\text{O}_2\text{CCF}_3)_2]_n$	— ^d	— ^a	— ^b	bpe	<i>rtt</i> -tpcb	1D → 2D	UV irradiation	60 h	41
20	$[\text{Cd}(1,3\text{-bdc})(4\text{-spy})_2]_n$	891655	$[\text{Cd}(1,3\text{-bdc})(4\text{-spy})(\text{HT-ppcb})_{0.5}]_n$	891656	4-spy	HT-ppcb HT-ppcb = 1,3-bis(4'-pyridyl)2,4-bis(phenyl)cyclobutane	1D → 2D	UV light	10 h	42
21, 22	$[\text{M}-(1,2\text{-chdc})(\text{bpe})_2(\text{H}_2\text{O})_2] \cdot \text{H}_2\text{O}$ M = Zn (21), Mn (22)	862847 Zn (21) 862848 Mn (22)	$[\text{M}-(1,2\text{-chdc})(\text{tpcb})(\text{H}_2\text{O})_2] \cdot \text{H}_2\text{O}$ M = Zn (21'), Mn (22')	862849 Zn (21') 862850 Mn (22')	bpe	tpcb	1D → 3D	Hg lamp (400 W)	11 h	43
23	$[\text{Zn}_2(\text{cca})_2(4\text{-spy})_2]$	829795	$[\text{Zn}_2(\text{cca})_2(\text{rtt}-4\text{-ppcb})]$	829796	4-spy	<i>rtt</i> -4-ppcb <i>rtt</i> -4-ppcb = 1,3-bis(4'-pyridyl)-2,4-bis(phenyl)cyclobutane	2D → 3D	UV Irradiation Xenon source	90 min	44
24	$[\text{Zn}_2(\text{ndc})_2(4\text{-spy})_2]$	829797	$[\text{Zn}_2(\text{ndc})_2(\text{rtt}-4\text{-ppcb})]$	— ^b	4-spy	<i>rtt</i> -4-ppcb	2D → 3D	UV irradiation Xenon source	90 min	44
25	$[\text{Zn}_2(\text{bdc})_2(2\text{F-4spy})_2] \cdot \text{MeOH}$	965945	$[\text{Zn}_2(\text{bdc})_2(\text{rtt}-\text{F-ppcb})]$	965946	2F-4spy	<i>rtt</i> -F-ppcb	2D → 3D	UV irradiation	150 min	45
26	$[\text{Zn}_2(\text{bdc})_2(4\text{-spy})_2] \cdot 0.5\text{MeOH}$	965947	— ^a	— ^b	4-spy	ppcb ppcb = <i>rtt</i> -1,3-bis(4'-pyridyl)-2,4-bis(phenyl)cyclobutane	2D → 3D	UV irradiation	120 min	45
27	$[\text{Mn}_2\text{L}_2(\text{H}_2\text{O})_2] \cdot 3\text{H}_2\text{O}$	808588	$[\text{Mn}_2\text{L}'(\text{H}_2\text{O})_2] \cdot 3\text{H}_2\text{O}$	808589	L	L' H ₄ L' = 5,5'-(3,4-diphenylcyclobutane-1,2-diyl)dii-sophthalic acid	2D → 3D	300 W Hg lamp irradiation	24 h	46

^a The molecular formula is not given in the original literature. ^b Some structures after transformation are not suitable for single-crystal X-ray diffraction analysis, so the CCDC number is not available in the original literature. ^c The structure of complex 5 was found to be isostructural to complex 3 as their powder XRD patterns match. ^d The CCDC refcode is not given in the original literature.



Scheme 2 Ligands mentioned in part 2 of SCSC transformations in the form of [2 + 2] photochemical reactions.

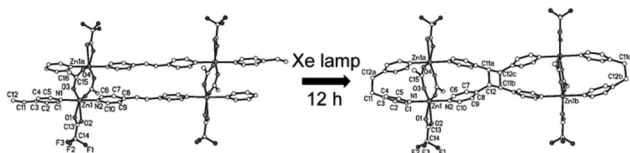


Fig. 1 View of the SCSC transformation that occurs in complex 1. Reprinted with permission from ref. 29. Copyright (2005) John Wiley and Sons.

irradiation for 5 h, a photoreaction of complex 2 was confirmed by the ^1H NMR spectrum, affording a new 1D double-chain polymer $[\text{Cd}(\text{rctt-tpcb})_{0.5}(\text{CBA})_2]_n$ (**2'**), as shown in Fig. 2.

In 2012, Vittal *et al.* described the synthesis, structural characteristics, and photoreactivity of three 2D coordination polymers, $[\text{Cd}_2(\text{pvba})_2(\text{tbdc})(\text{dmf})_2]_n$ (**3**, H_2tbdc = 2,3,5,6-tetrabromobenzene-1,4-dioic acid), $[\text{Co}_2(\text{pvba})_2(\text{tbdc})(\text{dmf})_2(\text{H}_2\text{O})_2]_n$ (**4**) and $[\text{Ni}_2(\text{pvba})_2(\text{tbdc})(\text{dmf})_2(\text{H}_2\text{O})_2]_n$ (**5**), which underwent photochemical reactions that appear to facilitate 2D to 2D structural transformations (Fig. 3).³¹ By being exposed to UV light for only 15 min, complex 3 underwent quantitative photodimerization to yield compound **3'**, which had a similar connectivity to the original one with the bcbpcb ligand (the HT-

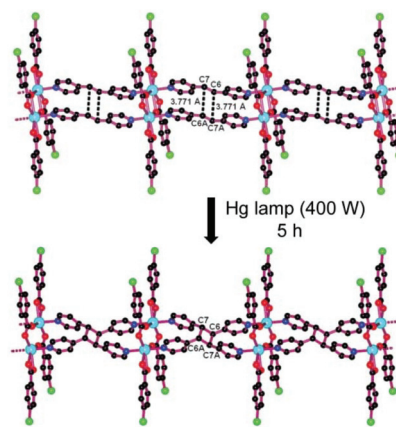


Fig. 2 View of the SCSC transformation that occurs in complex 2. Reprinted with permission from ref. 30. Copyright (2011) Royal Society of Chemistry.

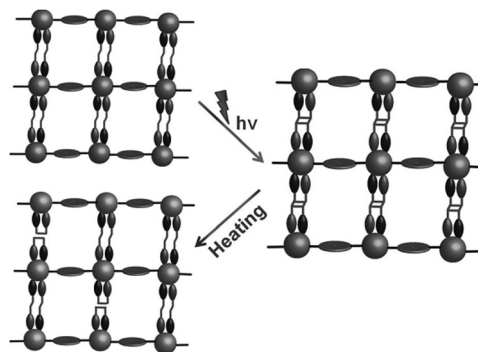


Fig. 3 Structural transformation of **3–5**, photodimerization under UV irradiation and cleavage by heat. Reprinted with permission from ref. 31. Copyright (2012) John Wiley and Sons.

dimer of pvba) instead of a pvba pair. Similarly, complex 4 and complex 5 underwent photodimerization upon irradiation like complex 3. These three transformations were all confirmed by ^1H NMR spectroscopic characterization. Furthermore, these [2 + 2] cycloaddition products can be reversed back to their monomers by using thermal means. After heat treatment, the cyclobutane rings were cleaved in two different ways to afford their corresponding ethylene derivatives. Although cleavage of cyclobutane derivatives into olefins by thermal means had been previously reported, cleavage in coordination polymers was reported for the first time in Vittal's paper.

In 2014, another kind of 2D to 2D [2 + 2] photochemical reaction was reported by Yang *et al.*³² The addition of a secondary organic ligand, 1,4-bpeb, to the reaction of 1,3-pda with Mn(II) facilitated the crystallization of a porous coordination polymer $[\{\text{Mn}(1,4\text{-bpeb})(1,3\text{-pda})\} \cdot (1,4\text{-bpeb})]_n$ (**6**), in which 1,4-bpeb plays the role of a ligand as well as that of a guest. In this research, the authors monitored the progress of the photoreaction in a step-by-step manner and produced a series of snapshots of the entire reaction process. IR spectroscopy of the powder samples and single-crystal X-ray diffrac-

tion of the crystal samples were carried out to trace every snapshot. Three reaction equilibria and three types of photochemical reactions (polymerization, dimerization, and pedal-like isomerization) were observed. The authors showed that when the UV energy is not very high, only the photoreaction of 1,4-bpeb in **6** occurred, and the 1,3-pda ligand became effectively photo-inert. When the radiation energy became higher, significant structural changes were observed with the guest and host 1,4-bpeb molecules. Both conformations of the 1,4-bpeb ligands in the channels decreased significantly when the sample was irradiated for 1 h, and this polymerization process is complete at 6 h (Fig. 4). Triggered by the polymerization, the host ligand 1,4-bpeb I form isomerized to the 1,4-bpeb II form and this isomerization converted back slightly as the irradiation time increased. Finally, the reaction yield was about 50%, and the author ascribes the reason behind the incomplete reaction to the structural constraints imposed by the guest polymer, which fills up the cavities and the ligand dimers, significantly distorting the coordination framework. On the other hand, during UV irradiation for 6 h, 1,3-pda remained intact with only minor changes induced by isomerization. These structural transformations can be explained by the fact that once a photochemical reaction is initiated by absorption of a UV photon, it triggers a chain of structural transformations that enable further photochemical reactions to occur. Throughout the reactions, the whole framework remained intact, although significantly distorted. This is the first instance of a solid-state regioselective $[2 + 2]$ polymerization and the first example of a coordination polymer where both ligands and guest molecules photoreact under UV irradiation.

In 2010, the first example of a 3D to 3D SCSC transformation in interpenetrated coordination polymers induced by UV light was reported by Vittal's group.³³ Three 3D complexes $[\text{Zn}(\text{bpe})(\text{muco})]\cdot\text{DMF}\cdot\text{H}_2\text{O}$ (**7**, H_2muco = *trans,trans*-muconic acid), $[\text{Zn}(\text{bpe})(\text{bdc})]\cdot\text{DMF}$ (**8**, H_2bdc = 1,4-benzene dicarboxylic acid) and $[\text{Zn}(\text{bpe})(\text{fum})]\cdot\text{H}_2\text{O}$ (**9**, H_2fum = fumaric acid), in which bpe ligand pairs act as pillars, all underwent 100% topochemical $[2 + 2]$ cycloaddition reactions in similar ways. Taking complex **7** as an example (Fig. 5), the two Zn(II) centers are bridged by two dicarboxylate ligands, and bpe pairs are aligned parallelly to form a ladder polymer. The distances between the centers of the adjacent C=C bonds meet the

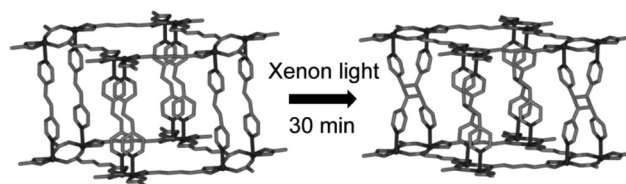


Fig. 5 A perspective view of one of the two independent distorted cubic nets in **7** before and after UV irradiation. Reprinted with permission from ref. 33. Copyright (2010) John Wiley and Sons.

requirements of a $[2 + 2]$ cycloaddition reaction. After being subjected to UV irradiation for 30 min, the ^1H NMR spectra demonstrated the complete conversion of this complex. Structure analysis showed that the connectivity of dicarboxylate ligands in **7** generates a distorted cubic ($\alpha\text{-Po}$) structure, which is large enough to be interpenetrated by a second cube. In order to obtain higher crystal quality, single crystals were irradiated at 223 K and crystal data before and after irradiation were also collected at the same temperature. In this manner, single-crystal X-ray analyses of $[\text{Zn}(\text{rctt-tpcb})_{1/2}(\text{muco})]\cdot\text{DMF}\cdot\text{H}_2\text{O}$ (**7'**) and $[\text{Zn}(\text{rctt-tpcb})_{1/2}(\text{bdc})]\cdot\text{DMF}$ (**8'**) revealed a 100% photodimerization reaction accompanied by SCSC transformation, and only the single crystal of the photodimerized product of **9** showed cracking.

Similar 3D to 3D transformations have been observed in the complexes $\{[\text{Zn}_4(\mu_3\text{-OH})_2(5\text{-sipa})_2(1,4\text{-bpeb})_2]\cdot 4\text{H}_2\text{O}\}_n$ (**10**, 5- H_3sipa = dicarboxylic acids 5-sulfoisophthalic acid), $\{\text{Cd}_2(1,3\text{-pda})_2(1,4\text{-bpeb})_2\}_n$ (**11**, 1,3- H_2pda = 1,3-phenylenediacetic acid) and $[\text{Zn}_2(\text{bpeb})(\text{bdc})(\text{fa})_2]$ (**12**, H_2bdc = 1,4-benzenedicarboxylic acid, fa = formate).^{34,35}

In 2017, Lang *et al.* reported an interesting 3D to 3D transformation from $[\{\text{Cd}(\text{ppene})(1,4\text{-BDC})\}\cdot\text{MeCN}]_n$ (**13**, 1,4- H_2BDC = 1,4-benzenedicarboxylic acid) to $[\{\text{Cd}_2(4\text{-tp-3-lad})(1,4\text{-BDC})_2\}\cdot 2\text{MeCN}]_n$ (**13'**) induced by UV irradiation and accompanied by increased performance in detecting explosives (Fig. 6).³⁶ The Cd ions in **13** adopt six-coordinated octahedral geometries giving a $[\text{CdO}_4\text{N}_2]$ cluster, which is further linked by 1,4-BDC and ppene ligands to afford a 3D framework. Each channel of the framework is big enough to accommodate another one to form a two-fold interpenetrating 3D framework. Samples of **13** were exposed to UV light (365 nm) for about 12 h. Single-crystal X-ray analysis confirmed that this $[2 + 2]$ cycloaddition process proceeds in an absolute SCSC manner, with both the morphology and transparent appearance maintained. Furthermore, the ^1H NMR spectra of the crystalline powder samples showed that the conversion from ppene to the 4-tp-3-lad ligand was in a quantitative yield. Each new cyclobutane ligand was still coordinated to the same metal centers. So, the whole structure of **13'** was almost retained, except for a slight change in the bond lengths. This UV product **13'** was then used to sense nitroaromatics based on fluorescence quenching. The results show that **13'** revealed a higher selectivity and sensitivity than that of **13** in the detection of nitroaromatics. In addition, the emission maximum wavelength of **13'** showed a linear relation with Hg^{2+} concentration, blue-shifted

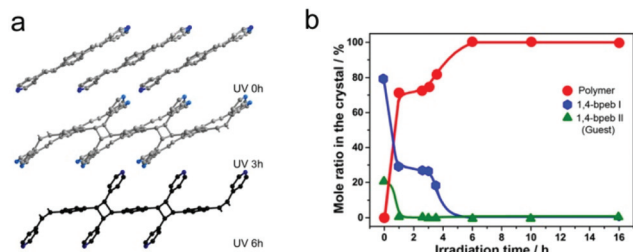


Fig. 4 Polymerization of 1,4-bpeb guest molecules in single crystals of **6** at different UV irradiation times. Reprinted with permission from ref. 32. Copyright (2014) American Chemical Society.

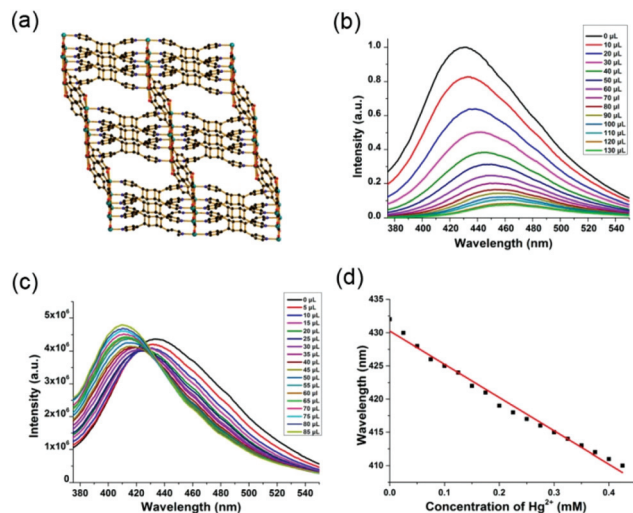


Fig. 6 (a) 3D single net of complex **13**. (b) Emission spectra of **13'** dispersed in water upon incremental addition of 2,4-DNP. (c) Emission spectra of **13'** dispersed in water upon incremental addition of Hg²⁺. (d) The relationship between the wavelength and the Hg²⁺ concentration. Reprinted with permission from ref. 36. Copyright (2017) American Chemical Society.

from 432 to 410 nm, which indicates that **13'** could be employed as a luminescent probe for sensing Hg²⁺. In summary, through this kind of [2 + 2] cycloaddition, a functional coordination polymer with fascinating photochemical performance was fabricated.

2.2 SCSC transformation induced by photodimerization with an increase in structural dimensions

The cycloaddition of C=C bonds brings about the formation of new chemical bonds, while also leading to changes in the whole structure. In order to fulfill the space requirements of cycloaddition, this kind of reaction is always accompanied by major movement and rotation of ions and ligands. Furthermore, this rearrangement and shrinkage always leads to an increase in the structure dimensionality.

In 2005, MacGillivray *et al.* reported a [2 + 2] photodimerization in the solid state by using silver ions, in the form of Ag(I), which resulted in a dimensionality increase from 0D to 1D.³⁷ The reaction of AgCO₂CF₃ and 4-stilbz afforded large colorless crystals of complex [Ag₂(4-stilbz)₄][CO₂CF₃]₂ (**14**). The structure, confirmed by single-crystal X-ray diffraction, showed that each Ag(I) ion in **14** is coordinated by two nitrogen atoms from two 4-pyridyl groups and one sphere oxygen atom from a carboxylate in a T-shaped geometry. The C=C bonds in this structure adopt a crisscross arrangement in the range of 3.8 Å, within the appropriate distance for a [2 + 2] photoreaction. When the crystals were exposed to UV radiation (broadband Hg lamp) for 18 h, [Ag₂(4-pyr-ph-cb)₂][CO₂CF₃]₂ (**14'**) was obtained (Fig. 7). The formation of the photoproduct was shown by the disappearance of the signals of the olefinic protons and the emergence of signals of the cyclobutane protons revealed in the ¹H NMR spectrum. Optical microscopy

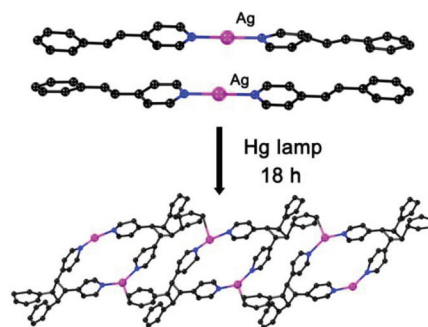


Fig. 7 Schematic illustration of the 0D to 1D SCSC transformation. Top: ball and stick picture of **14**; below: newly formed 1D coordination polymer. Reprinted with permission from ref. 37. Copyright (2005) John Wiley and Sons.

revealed that the single crystals remained intact, which suggests that this solid reaction underwent a SCSC transformation. This result was also confirmed by X-ray diffraction analysis. In order to generate 4-pyr-ph-cb, the Ag(I) and carboxylate ions underwent a degree of repositioning. An important consequence of this movement and rotation is that Ag–C bonds (Ag...C(phenyl) distance of 2.63 Å) were formed. Adjacent complexes of **14'** linked with each other to give a linear coordination polymer. This study represents the first case in which a finite metal complex has been transformed into a 1D infinite coordination network in the solid state *via* a [2 + 2] photoreaction.

As a continuation of the above-mentioned work, MacGillivray's group reported two similar 0D to 1D SCSC photodimerization reactions in two discrete dinuclear Ag(I) complexes: Ag₂(Cl-pyr-pe)₄(ClO₃)₂ (**15**) and [Ag₂(4-stilbz)₄][CF₃SO₃]₂ (**16**), as shown in Fig. 8.^{38,39} It is worth mentioning that the second transformation led to an obvious increase in the conductivity of the compound.³⁹ After photodimerization, the electrical conductivity of the new product, [Ag₂(4-pyr-ph-cb)₂][CF₃SO₃]₂ (**16'**), reached 37.0 ± 4.1 S cm⁻¹, an increase of approximately 40%. Density of states (DOS) cal-

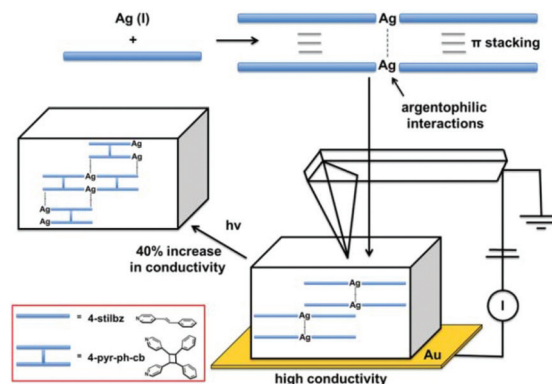


Fig. 8 Illustration of the SCSC [2 + 2] photodimerization and the conductivity experiment of complex **16** and **16'**. Reprinted with permission from ref. 39. Copyright (2014) American Chemical Society.

culations demonstrated this transformation at the same time. This is the first example of an increase in conductivity resulting from a [2 + 2] photodimerization.

In 2013, Medishetty's group designed and synthesized two isostructural Zn(II) complexes, $[\text{ZnBr}_2(4\text{-spy})_2]$ (**17**) and $[\text{ZnBr}_2(2\text{F-4spy})_2]$ (**18**), which both underwent a 0D to 1D [2 + 2] cycloaddition reaction in the SCSC manner reversibly.⁴⁰ Taking a single crystal of $[\text{ZnBr}_2(4\text{-spy})_2]$ (**17**) as an example (Fig. 9), after UV irradiation for 24 h, 50% of the 4spy ligands in **17** underwent a photochemical reaction resulting in the formation of the expected dimer, $[\text{Zn}_2\text{Br}_4(\text{rctt-ppcb})(4\text{-spy})_2]$ (**17'**). This result was monitored by single-crystal X-ray crystallography and ^1H NMR spectroscopy. Interestingly, heating the dimer **17'** at 220 °C for 48 h led to a complete reversible structural transformation from **17'** back to **17**. This was the first demonstration of such a reversible 0D to 1D structural transformation between metal complexes due to cyclobutane formation by UV light irradiation and its cleavage by heating. Further study indicated that the reactivity of the ground powder samples was very high and showed 50% conversion within 2 h of UV irradiation, due to the higher surface area exposed to UV light. By 60 h, all of the C=C bonds in 4spy were converted to the cyclobutane ring, and a new 1D polymer $[\text{ZnBr}_2(\text{rctt-ppcb})]$ (**17''**) formed. The dimers are presumed to be the stable intermediates in the formation of the 1D coordination polymer, as upon prolonged exposure to UV light, the final product was obtained. Similar reactions were observed with $[\text{ZnBr}_2(2\text{F-4spy})_2]$ (**18**). It is worth mentioning that the photoreactivity of a ground powder of **18** was even higher, with 80% conversion of C=C bonds within just 2 h. In other words, there was no intermediate dimer when crystal **18** was ground to a powder.

A 1D to 2D photo-polymerization was observed in 2010 in the cycloaddition reaction of a triple-stranded 1D coordination polymer $[\text{Pb}_3(\mu\text{-bpe})_3(\mu\text{-O}_2\text{CCH}_3)_2(\mu\text{-O}_2\text{CCF}_3)_4\{\text{O}_2\text{CCF}_3\}_2]_n$ (**19**), as illustrated in Fig. 10.⁴¹ Single-crystal X-ray crystallography revealed that **19** is a triple-stranded ribbon-like coordination polymer comprising three $[\text{Pb}(\text{bpe})]$ chains joined by CH_3CO_2^- and CF_3CO_2^- ligands. In the structure, the C=C bonds of the three polymeric strands are stacked parallelly and separated by

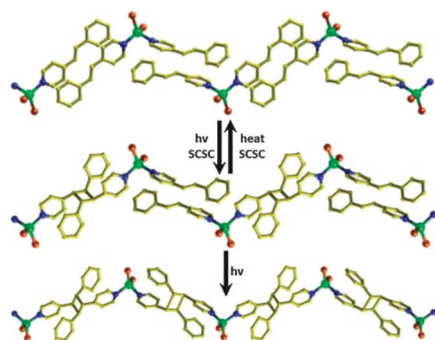


Fig. 9 Schematic diagram showing the reversible dimer formation of **17** and its polymerization to a 1D coordination polymer. Reprinted with permission from ref. 40. Copyright (2013) Royal Society of Chemistry.

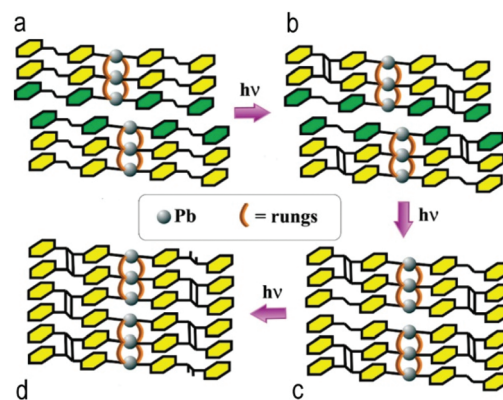


Fig. 10 The bpe ligands in the adjacent strands are shown in green. (a) Packing in **19**. (b) Random dimerization between the C=C bonds in each strand. (c) Reorganization at the end of the first step (67% conversion) to realign the remaining double bonds. (d) 100% photodimerized product. Reprinted with permission from ref. 41. Copyright (2010) American Chemical Society.

3.93 Å, suitable for a photodimerization reaction. The shortest distance between the C=C bonds in the adjacent polymers is 7.614 Å, which is too far away to be photochemically reactive. It is interesting to find that these single crystals react faster in the initial stage, producing the dimer in 67% yield after 1 h of UV irradiation and reaching 100% after 60 h. When the single crystals were ground to a powder and subjected to UV irradiation for a period of 1 h, only 40% photoconversion was observed. However, after a period of 40 h, 100% conversion was observed. In order to explain this unusual phenomenon, the mechanism has been proposed as follows. The 67% photodimerization is proposed to occur between the bpe pairs of the triple-stranded coordination polymer at first, and later by movements of the adjacent strands. A $\pi\cdots\pi$ interaction was established between the remaining 33% unreacted bpe pairs in the interstrands. After continuous UV irradiation, a 100% photodimerized product was obtained.

In 2013, Lang *et al.* reported another 1D coordination polymer, $[\text{Cd}(1,3\text{-bdc})(4\text{-spy})_2]_n$ (**20**, 1,3-H₂bdc = 1,3-benzenedicarboxylic acid), which could be converted to a 2D network $[\text{Cd}(1,3\text{-bdc})(4\text{-spy})(\text{HT-ppcb})_{0.5}]_n$ (**20'**) through a [2 + 2] photodimerization reaction (Fig. 11).⁴² X-ray analysis revealed that the

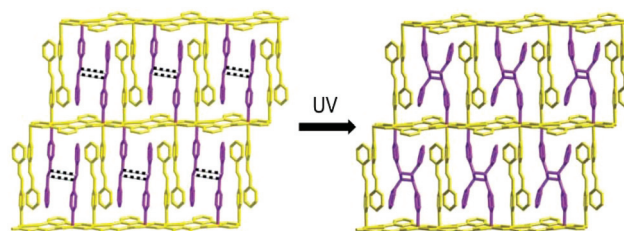


Fig. 11 [2 + 2] cycloaddition reaction induced by UV irradiation in **20** (HT-ppcb molecules formed from the [2 + 2] cycloaddition reaction are highlighted in purple). Reprinted with permission from ref. 42. Copyright (2013) Royal Society of Chemistry.

Cd(II) centers are linked by 1,3-bdc ligands to form a $[\text{Cd}(\text{bdc})]$ double chain. The 4-spy ligands are arranged in pairs, with each ligand bound to Cd(II) centers of the same double chain but belonging to different rows. In the extended structure, pairs of 4-spy ligands from neighboring chains interdigitate, exhibiting a “head-to-tail” arrangement. There are two crystallographically distinct 4-spy ligands, but only one of them exhibits close contact through the interdigitation. When single crystals of **20** were subjected to UV light for 10 h, X-ray analysis indicated that a photoinduced $[2 + 2]$ cycloaddition reaction had occurred, resulting in the dimerization of 50% of the 4-spy ligands to HT-ppcb in a SCSC transformation mode. The formation of new covalent bonds resulted in the conversion from 1D linear polymer **20** to a 2D network, $[\text{Cd}(1,3\text{-bdc})(4\text{-spy})(\text{HT-ppcb})_{0.5}]_n$ (**20'**). The formation of HT-ppcb ligand was supported by NMR studies.

In 2012, Tong *et al.* obtained two metal–organic frameworks, $[\text{M}(1,2\text{-chdc})(\text{bpe})_2(\text{H}_2\text{O})_2] \cdot \text{H}_2\text{O}$ ($\text{M} = \text{Zn}$ (**21**), Mn (**22**), 1,2-chdc = *trans*-1,2-cyclohexanedicarboxylate), which both underwent quantitative $[2 + 2]$ photodimerization in SCSC mode from 1D to 3D (Fig. 12).⁴³ The 1,2-chdc ligands, with two carboxylate groups connecting two zinc atoms in monodentate mode, act as bridges to form a 1D $\text{Zn}(1,2\text{-chdc})$ chain. Next, the bpe ligands adopt a monodentate coordination mode extending in four directions. The nonbonding distance of C=C bonds between two bpe ligands in the adjacent chains is 3.73 Å, which satisfies Schmidt's topochemical criteria. When single crystals of **21** were irradiated by a Hg lamp (400 W) for 11 h, colorless crystals of $[\text{Zn}(1,2\text{-chdc})(\text{tpcb})(\text{H}_2\text{O})_2] \cdot \text{H}_2\text{O}$ (**21'**) were obtained *via* a SCSC transformation. The complete cycloaddition of double bonds from bpe ligands was confirmed by single-crystal X-ray crystallography and IR spectroscopy. Since four directional bpe ligands in complex **21** were connected by the cycloaddition reaction, a 3D structure was formed in complex **21'**. This is the first example of a SCSC transformation from a 1D chain to a 3D framework through $[2 + 2]$ photodimerization.

In 2011, Vittal's group reported a classical photo-polymerization *via* a 2D to 3D $[2 + 2]$ cycloaddition in the SCSC manner (Fig. 13). Single-crystal X-ray structure determination at 100 K revealed that $[\text{Zn}_2(\text{cca})_2(4\text{-spy})_2]$ (**23**, H_2cca = 4-carboxycinnamic acid) is a 2D coordination polymer.⁴⁴ The building

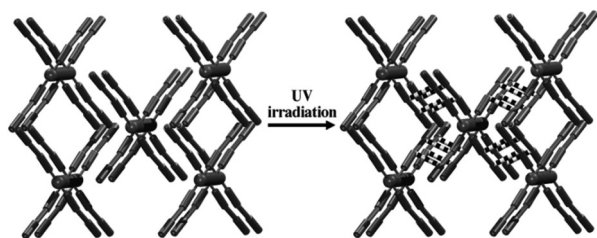


Fig. 12 Schematic diagram of the transformation from 1D staggered-sculs chains in **21** to 3D frameworks in **21'** through $[2 + 2]$ photodimerization. Reprinted with permission from ref. 43. Copyright (2012) John Wiley and Sons.

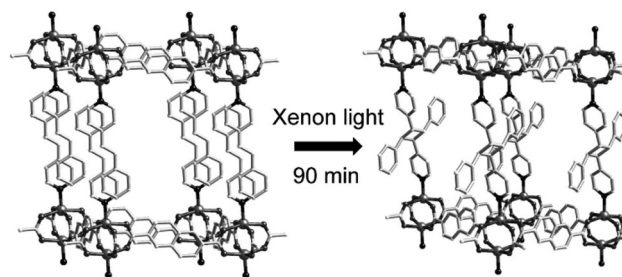


Fig. 13 $[2 + 2]$ cycloaddition of 4-spy ligands between the first and fourth layers of the 2D coordination polymer in the packing of **23**. Reprinted with permission from ref. 44. Copyright (2011) John Wiley and Sons.

block $[\text{Zn}_2(\text{cca})_2(4\text{-spy})_2]$ has the well-known $[\text{Cu}_2(\text{O}_2\text{CCH}_3)_4(\text{H}_2\text{O})_2]$ paddle-wheel structure. In each Zn(II) atom, the equatorial positions are coordinated by oxygen atoms of cca ligands and the axial position is occupied by the N atom of 4-spy to provide a 2D coordination polymer with an approximately square-grid structure. The 4-spy ligands of the fourth layers (one above and one below) are aligned exactly parallel to the 4-spy ligand in the top and bottom of the square grids. The alignment of the olefinic bonds between the 4-spy ligand pairs in the first and fourth layers exhibits a head-to-tail fashion and satisfies Schmidt's topochemical criteria (<4.2 Å) for a $[2 + 2]$ photochemical reaction. This situation provides an opportunity to conduct a structural transformation from interdigitated 2D layers into 3D interpenetrated structures. Single crystals of **23** were subjected to UV irradiation at room temperature by a Xenon source for 90 min. The ^1H NMR spectrum of the irradiated complex confirmed 100% conversion of 4-spy ligands into 1,3-bis(4'-pyridyl)-2,4-bis(phenyl)cyclobutane (*rcdt*-4-ppcb). Meanwhile, single-crystal X-ray analysis of the irradiated product $[\text{Zn}_2(\text{cca})_2(\text{rcdt-4-ppcb})]$ (**23'**) also revealed the formation of this triply-interpenetrated 3D coordination polymer with a primitive cubic topology. The complex $[\text{Zn}_2(\text{ndc})_2(4\text{-spy})_2]$ (**24**, H_2ndc = 2,6-naphthalenedicarboxylic acid) undergoes a similar 2D to 3D $[2 + 2]$ cycloaddition as **23**.

Similar 2D to 3D SCSC photo-polymerizations *via* $[2 + 2]$ cycloaddition were observed for complex $[\text{Zn}_2(\text{bdc})_2(2\text{F-4spy})_2] \cdot \text{MeOH}$ (**25**, bdc = 1,4-benzenedicarboxylic acid).⁴⁵ Single-crystal X-ray data confirmed the complete transformation of the 2D interdigitated structure of **25** into a doubly-interpenetrated 3D structure, $[\text{Zn}_2(\text{bdc})_2(\text{rcdt-F-ppcb})]$ (**25'**), by the quantitative $[2 + 2]$ cycloaddition reaction between the 2F-4spy ligand pairs aligned in a head-to-tail fashion (Fig. 14). The isostructural complex $[\text{Zn}_2(\text{bdc})_2(4\text{-spy})_2] \cdot 0.5\text{MeOH}$ (**26**) may well be predicted to be converted to a doubly-interpenetrated structure with α -Po topology similar to that of **25'**. Although no single-crystal X-ray data of **26'** was obtained, ^1H NMR spectral analysis was used to monitor this process.

Unlike the interpenetrated structures, Wu *et al.* reported another type of 2D to 3D SCSC UV-induced $[2 + 2]$ cycloaddition.⁴⁶ Complex $[\text{Mn}_2\text{L}_2(\text{H}_2\text{O})_2] \cdot 3\text{H}_2\text{O}$ (**27**, H_2L = *E*-5-(2-

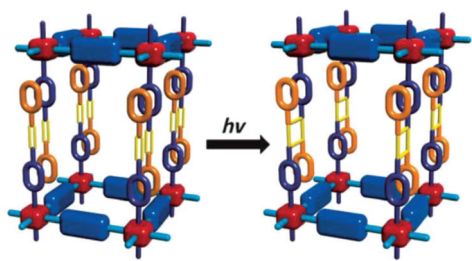


Fig. 14 Schematic diagram depicting the transformation of 2D interdigitated coordination polymer of **25** to 3D MOF of **25'**. Reprinted with permission from ref. 45. Copyright (2014) John Wiley and Sons.

(pyridin-4-yl)vinyl)isophthalic acid) exhibited a 100% photodimerization to $[\text{Mn}_2\text{L}'(\text{H}_2\text{O})_2]\cdot 3\text{H}_2\text{O}$ (**27'**), accompanied by a SCSC transformation. Topological analysis of **27'** revealed that the 3D network is an unusual (3,3,4,4)-connected tetranodal topology.

According to Schmidt's topochemical criteria for $[2 + 2]$ photochemical reactions, the distance between the two $\text{C}=\text{C}$ bonds must not exceed 4.2 Å. A $[2 + 2]$ photochemical cycloaddition reaction taking place in a coordination polymer is also confined to this law, and orientation matching of the $\text{C}=\text{C}$ bonds is also a crucial factor. As for complexes **1–5**, **7–9**, **13** and **19**, ligand pairs with $\text{C}=\text{C}$ bonds are always coordinated to one binuclear metal cluster, while being aligned parallelly at a relatively close distance. In this way, in rigid crystal structures the $\text{C}=\text{C}$ bonds are still reactive. The lengths of the $\text{C}=\text{C}$ bonds in the above-mentioned complexes are between 3.7 and 3.85 Å. As for complexes **6** and **14–18**, the original structures are zero dimensional, but the appropriate parallel stacking mode and the close distance allow the cycloaddition reactions to become a reality. The lengths of the $\text{C}=\text{C}$ bonds in these complexes are between 3.5 and 3.9 Å. In the case of the higher-dimensional structures, complexes **20–26**, the ligand pairs are usually aligned within different chains or layers, exhibiting a head-to-tail fashion, and in this way a photochemical reaction leads to an increase in the structure dimensionality. The $\text{C}=\text{C}$ bond lengths in these complexes range from 3.6 to 3.9 Å. In conclusion, as long as the orientation and distance are suitable, there is the possibility for a reaction. The distance range of ligands fixed in the skeleton is relatively small, while the range of free ligands is relatively wide.

3. SCSC transformation induced by loss/uptake of solvent vapor

Owing to the hydrothermal and solvent-thermal methods used in synthesizing coordination polymers, there are always many uncoordinated and coordinated water or solvent molecules in the pores of the structures. In most cases, the main framework remains unchanged during the removal of these molecules. This occurs on thousands of complexes but causes

no crystal structural transformations, so this aspect will not be deeply discussed in this review. In the other cases, the loss/uptake of solvent vapor brings breakage or generation of covalent bonds of the framework. We will discuss these examples in the following part in depth. On the one hand, loss/uptake of solvent vapor may lead to partial change of the skeleton; on the other hand, during the solvent vapor removal, structural transformation happens, which is accompanied by a change of the entire structure, such as an increase or decrease in dimensionality, polymerization and certain other changes.

Owing to the evacuation effect that happens in some desolvation processes, parts of the super-molecule start to move. When shrinkage is achieved to a certain extent, the original chemical bonds change, and this causes the rearrangement of the whole structure. In this way, new covalent bonds are created, and the dimensionality of the framework increases, which is accompanied by the loss of lattice solvent molecules or coordinated solvent molecules. In the following section, we will divide solid-state transformations induced by removal/uptake of solvent molecules into two sections: 3.1 Solvent vapor-induced partial structure change of the framework and 3.2 Solvent vapor-induced drastic structure change of the framework.

3.1 Solvent vapor-induced partial structural change of the framework

In many porous frameworks, there exists a variety of guest molecules in the channels, such as free solvent molecules, guest metal ions, guest ligand molecules and so on. Generally, these guest molecules have no strong coordination interaction with the framework, so removing or exchanging these molecules can be achieved by just heating or through molecule exchange. However, this kind of process also sometimes involves breakage and formation of covalent bonds, which will be discussed in the following section.

In 2011, Sun *et al.* reported a SCSC transformation upon removing non-coordinated and coordinated water molecules.⁴⁷ X-ray crystallographic analyses revealed that $\text{Co}(\text{II})$ in complex $[\text{Co}_3(\text{L}^1)_2(\text{BTEC})(\text{H}_2\text{O})_2]\cdot 2\text{H}_2\text{O}$ (**28**, $\text{HL}^1 = 3,5\text{-di}(\text{imidazol-1-yl})\text{benzoic acid}$, $\text{H}_4\text{BTEC} = 1,2,4,5\text{-benzenetetracarboxylic acid}$) is six-coordinated, exhibiting an octahedral coordination geometry. Three Co atoms are linked together by four $\mu_2\text{-O}_{\text{carboxyl}}$ atoms to form a $\text{Co}_3(\text{OCO})_6$ linear tri-nuclear secondary building unit (SBU). Each L^{1-} ligand links three SBUs using its two imidazole groups and one carboxylate group to form an infinite 2D (3,6)-connected **kgd** network. Furthermore, the 2D networks are further connected by BTEC^{4-} ligands to form a 3D binodal (3,8)-connected **tfz-d** framework. Two coordinated and two non-coordinated water molecules per formula unit are located within the channels and bear extensive hydrogen-bonding interactions with the framework. A two-step weight loss of complex **28** was observed in the thermogravimetric curve, which can be attributed respectively to the loss of non-coordinated and coordinated water molecules. When crystal samples of **28** were heated at 160 °C for 2 h, one coordinated water molecule of one $\text{Co}(\text{II})$ ion was lost. The coordination

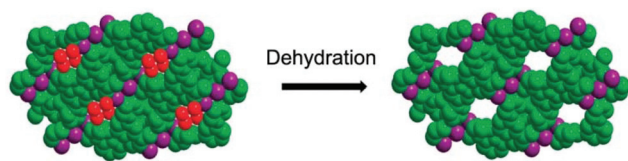


Fig. 15 Transformation of the coordination environment of Co(II) atoms in complex **28**. Reprinted with permission from ref. 47. Copyright (2014) American Chemical Society.

geometry of Co changed from octahedral to square pyramid, which was accompanied by a crystal color change from red to dark-violet. The color-change phenomenon is a general indication of the change in coordination environment of the Co(II) ions. Single-crystal X-ray diffraction of the dark-violet crystal confirmed that a dehydrated product, $[\text{Co}_3(\text{L}^1)_2(\text{BTEC})]$ (**28'**), was obtained with retention of crystallinity (Fig. 15). Moreover, the PXRD pattern of **28** activated at 160 °C is in good agreement with that of the as-synthesized sample, indicating the stability of the framework.

Some other examples showing similar dehydration processes have been reported by Zeng,⁴⁸ Ghosh,⁴⁹ Cheng,⁵⁰ Su,⁵¹ Dong⁵² and other researchers.^{53–55}

In addition to the changes in the metal geometries, the organic linkers can also undergo transformations. In 2013, an example of water elimination from across the ligand was described by Zeng and Kurmoo *et al.*⁵⁶ Firstly, upon heating to 120 °C, $\{\text{Zn}_3[(\text{L}^2)_2(\mu_2\text{-OH})_2]\cdot 6\text{H}_2\text{O}\}_n$ (**29**, $\text{H}_2\text{L}^2 = 2\text{-(1-hydroxyethyl)-1H-benzo[d]imidazole-5-carboxylic acid}$) underwent a SCSC transformation to form a guest-free framework (Fig. 16). Next, the free hydroxyethyl group ($-\text{CHOHCH}_3$) in the channels of **29** was modified to a vinyl group ($-\text{CH}=\text{CH}_2$) upon further heating to 250 °C. ¹H NMR results confirmed the existence of the vinyl group in this complex, and meanwhile, the integrity of the carbon backbone after this transformation was confirmed by PXRD patterns and ¹³C NMR spectra. Furthermore, this post-synthetic modification (PSM) method affords an organic complex that is difficult to prepare *via* traditional organic synthesis.

In 2014, Cheetham *et al.* described another example of this kind of transformation: the topotactic dehydration of a non-porous 3D MOF $[\text{Li}_2(\text{L}-\text{C}_4\text{H}_4\text{O}_5)]$ (**30**).⁵⁷ Upon heating to 280–350 °C, large single crystals of **30** produce a new mixed-ligand MOF, $[\text{Li}_2(\text{L}-\text{C}_4\text{H}_4\text{O}_5)_{1-x}(\text{C}_4\text{H}_2\text{O}_4)_x]$ (**30'**), while keeping themselves intact. The new structure was determined by

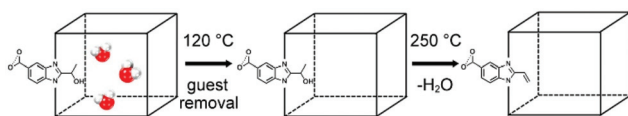


Fig. 16 Transformations of complex **29**: post-synthetic elimination of H_2O from the hydroxyethyl groups in the channels to form vinyl groups. Reprinted with permission from ref. 56. Copyright (2013) John Wiley and Sons.

single-crystal X-ray diffraction. During this transformation, the water was removed from the C–C bond in a stereospecific manner. MAS-NMR spectra, ¹H NMR spectra, ¹³C NMR spectra and FTIR spectra of **30'** demonstrated the above observations.

3.2 Solvent vapor-induced drastic structure change of the framework

Early in 2005, Chen's group reported a guest desorption/absorption-triggered 3D net rearrangement between 5-fold and 6-fold interpenetration (Fig. 17).⁵⁸ In complex $[\text{Ag}_6\text{Cl}(\text{atz})_4]\text{OH}\cdot 6\text{H}_2\text{O}$ (**31**, Hatz = 3-amino-1,2,4-triazole), if atz ligands are defined as 3-connected nodes and Ag(I) atoms are defined as linkers, then the whole framework represents a 3-connected 4.14² (**dia-f**) net. There are large holes existing in the frameworks, so five identical 3D single nets interlocked with each other to give a 5-fold interpenetrated structure. Its openings along the *a*- and *b*-directions are fully occupied, but there are still large 1D columned channels in the *c*-direction that accommodate guest molecules. When this complex was cooled to 103 K, tetragonal **31** was transformed into orthorhombic **31'** (*Fddd*), while the whole framework was kept intact except that the channels of **31'** are slightly elliptical. Upon heating to 293 K, this transformation could occur reversibly. In order to further study the effect of the guest molecules, the crystals were placed in a very slow stream of dry air, and a partially desolvated product $[\text{Ag}_6\text{Cl}(\text{atz})_4]\text{OH}\cdot x\text{H}_2\text{O}$ (**31''**, $x \leq 2$) was formed. **31''** crystallized in a new space group but the **dia** topology of the net was retained. However, the $\text{Ag}_3(\text{atz})_2$ nets in **31''** exhibit a 6-fold interpenetrating structure. Obviously, this means that the transformation from **31** to **31''** not only causes distortion of the nets but also the cleavage and formation of Ag(I)–ligand bonds. This transformation can be ascribed to the rearrangement of the linear Ag(I) ions of **31**, in which the OH^- or H_2O guests may coordinate to these Ag(I) ions to generate an intermediate structure. Furthermore, **31''** could be reversely converted back to **31** upon exposing the crystals to saturated water vapor.

This kind of guest-induced whole structural rearrangement was also found in complex $\{[\text{Cu}(\text{iba})_2]\cdot 2\text{H}_2\text{O}\}_n$ (**32**, iba = 4-(1H-imidazol-1-yl)benzoate) and $[\text{Zn}_2(\text{ndc})_2(\text{bpy})]$ (**33**, ndc = naphthalene dicarboxylic acid, bpy = 4,4'-bipyridine).^{59,60} The interpenetrating characteristics of these two complexes were changed by the removal of the guest molecules present in the channels, and these transformations also occur in a SCSC

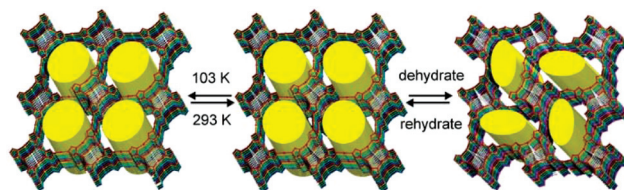


Fig. 17 Interconversion of the $[\text{Ag}_6\text{Cl}(\text{atz})_4]$ host of **31**, **31'** and **31''** (1D channels are highlighted as yellow columns). Reprinted with permission from ref. 58. Copyright (2005) American Chemical Society.

manner. Unlike the others, the very slow but spontaneous SCSC structural transformation from $\{[\text{Cu}(\text{iba})_2] \cdot 2\text{H}_2\text{O}\}_n$ (**32**) to $[\text{Cu}(\text{iba})_2]_n$ (**32'**) shows a loss of the entanglement characteristics.

In 2014, an interesting structural transformation induced by solvent removal was reported by Su and Lan *et al.* In this work, the centrosymmetric complex $[(\text{Zn}_4\text{O})_2(\text{L}^3)_3] \cdot 10\text{H}_2\text{O} \cdot 46\text{DMA}$ (**34**, H_4L^3 = methanetetra(tetrakis[4-(carboxyphenyl)oxamethyl]-methane acid)) was transformed into a chiral framework $[(\text{Zn}_4\text{O})_2(\text{L}^3)_3\text{H}_2\text{O}] \cdot \text{H}_2\text{O} \cdot 4\text{DMA}$ (**34'**) triggered by temperature and time simultaneously, without any solvent (Fig. 18).⁶¹ First, complex **34** was transformed into **34'** by simple heating in solvent with no dissolving or recrystallizing of any crystals. Next, in order to achieve this SCSC transformation in a solvent-free mode, a single crystal of **34** was sealed in a 0.8 mm diameter melting-point tube without solvent and heated at 140 °C for 72 h. The PXRD results indicated that the resulting samples match the simulated pattern of **34'** very well, proving that the SCSC transformation from **34** to **34'** was successfully realized. The detailed structural changes of this transformation have been proposed as follows. During the temperature increase, the solvent molecules move faster in the channels, which results in the partial coordination bonds of unstable **34** breaking. Then different $\text{Zn}_4\text{O}(\text{CO}_2)_6$ SBUs move closer to each other and coordinate with the water molecules to form new $[\text{Zn}_4\text{O}(\text{CO}_2)_6]_2\text{H}_2\text{O}$ SBUs, which recombine to generate the new complex **34'** in a certain period of time. Complex **34** is a kinetic product, formed easily from the components at relatively low temperature. With time and temperature increasing, this unstable product progressively converts to the thermodynamic product **34'**. Density functional theory (DFT) calculations also confirmed the better thermodynamic stability of complex **34'**, which matches well with the air stability experiments. This is the first report of a non-interpenetrated structure transforming into a self-penetrated structure without any solvent. In addition, the air-stable **34'** exhibits a more excellent gas adsorption ability than **34**.

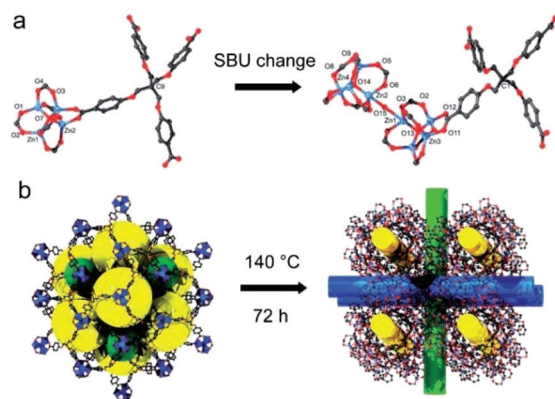


Fig. 18 SCSC transformation from an achiral MOF **34** into a chiral MOF **34'**, (a) SBU change, (b) framework change. Reprinted with permission from ref. 61. Copyright (2014) Royal Society of Chemistry.

In 2015, the work of Zhang *et al.* highlighted another crucial factor of structural reconstitution in SCSC transformations: the impact of ligand substituent groups.⁶² A series of isostructural 5-fold interpenetrated MOFs $[\text{Ag}_6(\mu_8\text{-X})(\text{Rtz})_4] \cdot \text{OH} \cdot 6\text{H}_2\text{O}$ (**35–38**, X = Cl, Br; Rtz = atz[−] or mtz[−], Hatz = 3-amino-1,2,4-triazole, Hmtz = 3-methyl-1,2,4-triazole) with different organic and inorganic components were successfully synthesized. Upon dehydration, **35** and **37** with $-\text{NH}_2$ groups changed to 6-fold interpenetration, while **36** and **38** with $-\text{CH}_3$ groups maintained their 5-fold interpenetrating framework, which was accompanied by only simple framework breathing (Fig. 19). This means that by altering the substituent groups exposed on the pore surface, the crystals underwent different reconstitution processes. The hydrophilic and hydrophobic properties of the substituent groups decide the distance between the guests and the Ag(I) centers, control the guest accessibility to the open metal sites, and further influence the cleavage and reformation of Ag–N coordination bonds during the rearrangement of the interpenetration. This work demonstrated that the actions of cleavage/formation of coordination bonds and interpenetration reconstitution can be allowed or suppressed by changing the ligand substituent group.

In addition to structural rearrangement caused by lattice water molecule removal, desolvation of coordinated water molecules can also lead to structural transformations. Early in 2007, Kitagawa *et al.* reported two complexes based on Mn(II) Cr(III) and Ce that both underwent 2D to 3D SCSC transformations induced by loss of solvent molecules (Fig. 20).^{63a,b} In 2010, Demadis *et al.* demonstrated a topotactic transformation from a 1D hybrid $[\text{Cu}(\text{HPAA})(\text{H}_2\text{O})_2] \cdot \text{H}_2\text{O}$ (**39**, HPAA = $\text{HO}_3\text{PCH}(\text{OH})\text{CO}_2$, hydroxyphosphonoacetate dianion) to an anhydrous 3D framework Cu(HPAA) **39'** via a pure desolvation process.^{63c} The room-temperature XRPD pattern of complex **39** starts to change at 30 °C, indicating the formation of a new phase: the

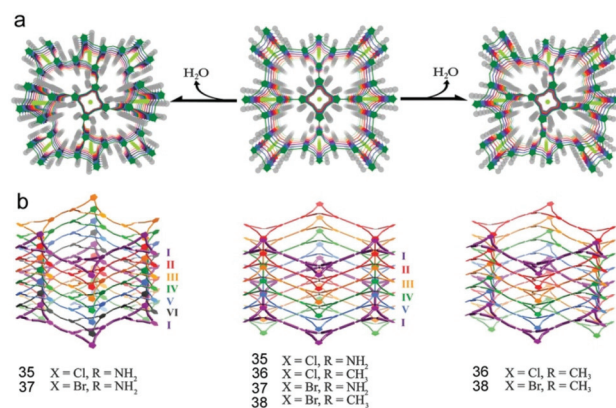


Fig. 19 Induced loss of solvent vapor, drastic framework breathing of a series of isostructural interpenetrated MOFs **35–38**, with (left) or without (right) 5- to 6-fold interpenetration reconstitution, controlled by the ligand substituent group. (a) Perspective views of 2×2 repeating units along the channel direction. (b) Perspective views perpendicular to the channel direction. Reprinted with permission from ref. 62. Copyright (2015) Royal Society of Chemistry.

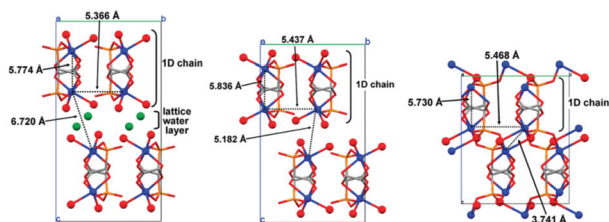


Fig. 20 Changes in packing between the 1D zigzag chains upon removal of the lattice water molecules and subsequent removal of Cu-bound water molecules (**39** left, **39'** middle, **39''** right). Reprinted with permission from ref. 63c. Copyright (2010) American Chemical Society.

1D intermediate $\text{Cu(HPAA)(H}_2\text{O)}_2$ **39'**. This removal of lattice water meanwhile results in alterations in hydrogen bonding interactions, which in turn leads to compaction of the chains as well as “slipping”. These changes contribute to the creation of new hydrogen bonds between the phosphonate groups and the hydroxyl/carboxy moieties. When the temperature increases to 70 °C, the initiation of the final step of the dehydration process occurs, which is accompanied by the appearance of new diffraction peaks. After the loss of the coordinated water molecules on Cu at 110 °C, the conversion from **39** to the final phase **39''** is complete. In this new 3D structure, the vacant sites on Cu *via* desolvation are finally occupied by oxygen atoms of phosphonate from neighboring chains, giving an axially-elongated octahedral environment. However, the topotactic transformation of a 1D hybrid to a 3D framework is thoroughly completed.

Structural transformations during activation are sometimes accompanied by the loss of the single-crystal integrity. Owing to the poor crystallinity of some samples after activation, structures cannot be determined directly by single-crystal XRD, and scientists use various methods to confirm the resulting structures. Although there is no single-crystal data, their high crystallinity makes it possible to obtain the corresponding structure from the PXRD curves. The Rietveld method is a common means to determine the final structure using PXRD patterns. For example, the crystal structure of **39''** discussed above was solved using the program EXPO2004 in the default setting, which gave all atoms present in the asymmetric unit. The structural model obtained was refined by the Rietveld method, with the GSAS package, and using soft constraints to maintain chemically reasonable geometries for the phosphonate and carboxylic groups. This kind of method has been widely used to determine the final structure of metal–organic frameworks with poor crystallinity. Another means to confirm the resulting structure after transformation is to synthesize the same structure in other ways, such as the situation for complex **34** and that of the following case. In 2013, $(\text{UO}_2)\text{Cu}(\text{H}_2\text{O})_2(\text{btcc}) \cdot 4\text{H}_2\text{O}$ (**40**, btcc = pyromellitate) was synthesized by Loiseau *et al.*, and its activated form $(\text{UO}_2)\text{Cu}(\text{btcc})$ (**40'**) was obtained either by heating **40** at 100 °C, or through hydrothermal synthesis at 200 °C, yielding single crystals that were suitable for structure determination.⁶⁴

Studies have shown that the loss of coordinated solvent molecules not only alters the characteristics of structures, but also largely affects the magnetic properties of a given complex. In 2010, the work of Sato *et al.* described such a change in magnetic properties caused by solvent removal.⁶⁵ Molecular magnets are becoming more and more attractive recently for their potential applications as switches and sensors. Connecting discrete magnetic motifs into an extended network is expected to bring more drastic magnetism changes. Changes in coordination number, geometry and the weak interactions between the guest molecules and the skeleton can dramatically modulate the magnetic properties of a coordination polymer. Tuning the magnetic behavior of coordination polymers using guest molecules is a fascinating topic. Chen's group, Coronado *et al.*, Zhang *et al.* and Cheng *et al.* have performed a lot of excellent work in this field, and other researchers have also made many contributions.⁶⁶ In 2010, Sato reported a reversible conversion from a hexanuclear cluster $[\{\text{Fe(III)}(\text{Tp})(\text{CN})_3\}_4\{\text{Co(II)}(\text{CH}_3\text{CN})(\text{H}_2\text{O})_2\}_2] \cdot 10\text{H}_2\text{O} \cdot 2\text{CH}_3\text{CN}$ (**41**, Tp = hydrotris(pyrazolyl)borate) to a 1D double-zigzag chain *via* a dehydration and rehydration process, which was accompanied by a drastic change in the magnetic behavior.⁶⁵ After slowly heating at 150 °C under a N_2 atmosphere, crystal data of the desolvated $[\text{Fe(III)}(\text{Tp})(\text{CN})_3]_2\text{Co}^{\text{II}}$ (**41'**) were successfully obtained from the single-crystal XRD measurements. The results revealed that **41'** crystallized in the *Ibam* space group. As shown in Fig. 21, during the transformation from **41** to **41'**, all uncoordinated and coordinated solvent molecules were lost. Simultaneously, the hexanuclear units moved towards each other and one of the terminal CN^- anions of monodentate $[\text{Fe}(\text{Tp})(\text{CN})_3]^-$ became coordinated to the nearest Co(II) in the neighboring hexanuclear unit. The distance between the Fe(III) in $[\text{Fe}(\text{Tp})(\text{CN})_3]^-$ and the nearest Co(II) in the neighboring hexanuclear unit was reduced to 5.051 Å after the formation of the coordination bonds, while it was 11.634 Å in **41**. In this way, the hexanuclear units in **41** linked one by one, forming a neutral double-zigzag chain. Each chain was further connected with four neighboring chains through the interlocked pyrazolyl rings of the $[\text{Fe}(\text{Tp})(\text{CN})_3]^-$ units, forming a 1D hexagonal channel along the *c* direction. This example clearly showed that conversion from a nonporous cluster to a MOF with nano-sized open channels was successfully achieved by a pure solid-state reaction. Surprisingly, this transformation was reversible. The reverse process from **41'** to **41** could be

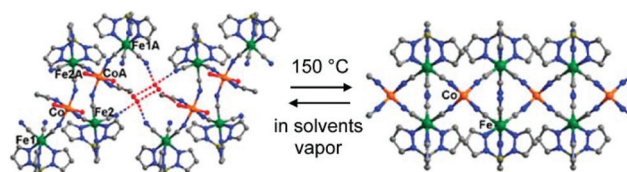


Fig. 21 Left, side view of the chain formed by hexanuclear units and a $(\text{H}_2\text{O})_4$ ring through the hydrogen bonds in **41**. Right, side view of the 1D double-zigzag chains in **41'**. Reprinted with permission from ref. 65. Copyright (2010) American Chemical Society.

easily induced by simply exposing **41'** to solvent vapor to release the strain energy. It is worth mentioning that the structure of **41'** cannot be obtained through reactions under other conditions. Accompanying the structural conversion, great changes occurred in the magnetic behavior. The interaction between Fe(III) and Co(II) in **41** was antiferromagnetic, whereas in **41'**, this interaction became ferromagnetic. Moreover, the χT value at room temperature changed from $9.0 \text{ cm}^3 \text{ K mol}^{-1}$ for **41** to $7.4 \text{ cm}^3 \text{ K mol}^{-1}$ for **41'**.

Such kind of transformation induced by desolvation with a change in magnetic properties was reported by Liu *et al.* in 2015⁶⁷ and Wen *et al.* in 2017.⁶⁸ In Liu's work, a 1D complex $[(\text{CuL}^{4.5}\text{H}_2\text{O})\cdot\text{H}_2\text{O}]_n$ (**42**, $\text{H}_4\text{L}^4 = 2,2'$ -bipyridine-3,3',6,6'-tetracarboxylic acid) underwent an irreversible SCSC transformation to generate a 3D anhydrous complex $[\text{CuL}^{4.5}]_n$ (**42'**) due to loss of water molecules. The antiferromagnetism of **42** changed to weak ferromagnetism in **42'** due to the new chemical bond bridge. In Wen's work, a 2D Gd(III)-based framework $[\text{Gd}(\text{pda})(\text{ox})_{0.5}(\text{H}_2\text{O})_2]_n$ (**43**, $\text{H}_2\text{pda} = \text{propanedioic acid}$, $\text{H}_2\text{ox} = \text{oxalic acid}$) changed to a 3D pillar-layer structure $[\text{Gd}(\text{pda})(\text{ox})_{0.5}]_n$ (**43'**), accompanied by a capacity rise in the magnetocaloric effect. The magnetic testing results indicated that **43'** could be regarded as an attractive cryogenic magnetorefrigerant.

The loss of water molecules always leads to changes in metal coordination geometry. The vacant coordination position of the metal is then occupied by other atoms in the structure, resulting in a dimensionality increase from the low to the high. As discussed above, not only do the structures change, but the properties of these compounds change a lot too. Aside from the most common changes in magnetic properties, coordination geometry variation also affects the proton conductivity of a complex. In 2016, Zheng *et al.* reported such a proton conductivity change by means of a SCSC process.⁶⁹ All examples discussed above widen the range of property applications enhanced by SCSC transformations.

Polyrotaxanes, based on coordinative bonds or $\pi\cdots\pi$ interactions with various dimensionalities have been recognized as a new type of coordination architecture. Removal of solvent molecules brings unexpected changes to this kind of complex. In 2010, Tzeng *et al.* reported a novel transformation from a 1D double-zigzag framework $\{[\text{Zn}(\text{paps})_2(\text{H}_2\text{O})_2](\text{ClO}_4)_2\}_n$ (**44**, $\text{paps} = N,N'$ -bis(pyridylcarbonyl)-4,4'-diaminodiphenyl thioether) to a 2D polyrotaxane framework $[\text{Zn}(\text{paps})_2(\text{ClO}_4)_2]_n$ (**44'**) by simply heating (Fig. 22).⁷⁰ Complexes **44** and **44'** can be obtained in the presence or absence of water in the reaction media, respectively. Both of their final structures were determined by single-crystal X-ray diffraction. In **44**, the Zn(II) atoms are coordinated by four N atoms from four paps ligands, and two water molecules in the axial positions to give a double-zigzag chain structure with a rhombohedral molecular square in the middle. After heating to 300°C , the Zn(II) ions lost their two coordinated water molecules, whereas ClO_4^- in the crystal lattice coordinated to the vacant Zn(II) ions. Meanwhile, the double-zigzag framework of **44** underwent an interlocking of the 1D rhombohedral molecular square, through nonclassical

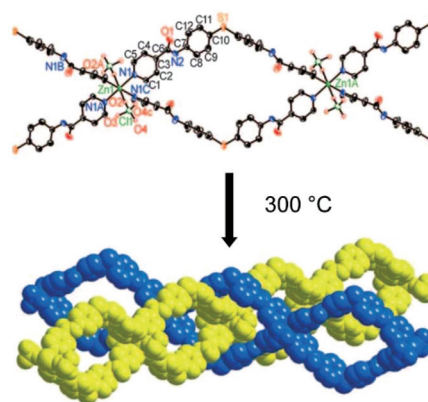


Fig. 22 1D double-zigzag framework **44** transformed into an interlocking structure **44'**. Reprinted with permission from ref. 70. Copyright (2010) John Wiley and Sons.

hydrogen interactions, generating a novel 2D polyrotaxane framework. The coordination environment of Zn(II) ions in **44'** is similar to that of **44**, except the two axial positions are changed to ClO_4^- anions. Variable-temperature PXRD patterns demonstrated that **44'** could be reversibly inter-converted. By grinding in the presence of moisture, water molecules displaced the ClO_4^- anions, facilitating the phase transformation back to the original state. In 2012, by changing the ligand paps to papo and papc, Tzeng's group described another two identical transformations just like the transformation from **44** to **44'**.⁷¹

In 2012, Kim *et al.* reported a transformation from a single 3D MOF, $[\text{Zn}_7\text{O}_2(\text{NBD})_5(\text{DMF})_2]_n$ (**45**, $\text{NBD} = 2\text{-nitrobenzene-1,4-dicarboxylate}$), to a doubly-interpenetrating form, $[\text{Zn}_7\text{O}_2(\text{NBD})_5]_n$ (**45'**), triggered by the removal of DMF molecules (Fig. 23).⁷² Each SBU $[\text{Zn}_7\text{O}_2(\text{CO}_2)_{10}(\text{DMF})_2]_n$ in **45** is connected by ten NBD linkers to give a **fqr** net. Two DMF molecules coordinating to two different Zn centers protrude themselves into the pores, acting as terminal ligands. After desolva-

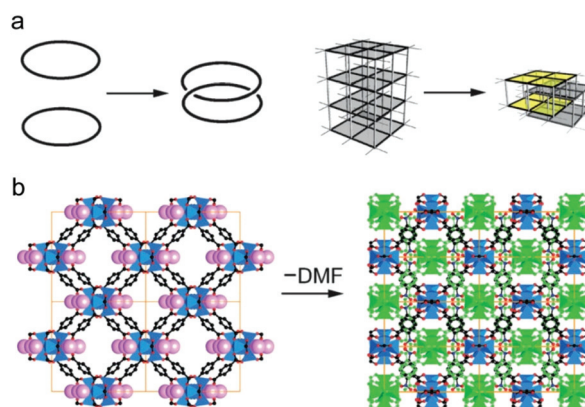


Fig. 23 (a) Catenation processes in molecules (left) are observed in three-dimensional MOFs (right). (b) **45** converts into the interpenetrated crystals of **45'** by the removal of coordinated DMF. Reprinted with permission from ref. 72. Copyright (2012) John Wiley and Sons.

tion, complex **45'** was obtained. Single-crystal X-ray diffraction analysis revealed that the coordination fashion of the central Zn atom changed from six-coordinated to four-coordinated after removal of the coordinated DMF molecules. Thus, each single framework of **45'** has a window that is big enough to accommodate a second one to generate a doubly-interpenetrated framework. Variable-temperature powder X-ray diffraction (PXRD) and gas adsorption measurements were also performed to confirm this transformation.

In the opposite direction of desolvation, uptake of solvent molecules by the metal cluster under an ambient atmosphere can also lead to SCSC transformations. In 2013, Bu reported the first example of a self-penetrating to interpenetrating topology transformation under ambient atmosphere triggered by hydration. Complex $[\text{Co}_{1.5}(\text{tipb})(\text{SO}_4)(\text{pta})_{0.5}](\text{DMF})_{1.75}$ (**46**, $\text{tipb} = 1,3,5\text{-tris}(\text{pimidazol-ylphenyl})\text{benzene}$, $\text{H}_2\text{pta} = \text{terephthalic acid}$) was successfully synthesized as blue block crystals with a self-penetrating structure.⁷³ This self-penetrating framework comprises two identical interpenetrating nets, which are further linked by pta^{2-} ligands. When the crystal was exposed to the air, a SCSC transformation occurred. H_2O ligands displaced pta^{2-} ligands, leading to a change in the coordination configuration of the $\text{Co}(\text{II})$ ions from tetrahedral to octahedral, and a 2-fold interpenetrating framework $[\text{Co}_{1.5}(\text{tipb})(\text{SO}_4)(\text{H}_2\text{O})_{3.6}](\text{pta})_{0.5}(\text{solvent})_n$ (**46'**) was formed (Fig. 24). The dissociation of pta^{2-} ligands from the framework led **46'** to exhibit micro-pores along the c axis, and the self-penetrating framework was split into two interpenetrating identical networks. By comparing the crystal structures of **46** and **46'**, the driving force behind the structural transformation can be attributed to the presence and coordination force of the H_2O molecules. The coordinated H_2O molecules in **46'** could be removed by heating or other methods to give **46** again. There was also a color change accompanying this reversible SCSC transformation and this structure transformation could also be triggered by NH_3 .

In 2014, Du *et al.* reported another fantastic transformation accompanied by a change in entanglement characteristics.⁷⁴ In the entangled structure of complex $[\text{Cu}(\text{tba})_2]_n$ (**47**, $\text{Htba} = 4\text{-(1H-1,2,4-triazol-1-yl)benzoic acid}$), each $\text{Cu}(\text{II})$ ion is coordinated by two carboxylate oxygen atoms and two triazolyl nitrogen atoms. The adjacent $\text{Cu}(\text{II})$ centers are linked by tba

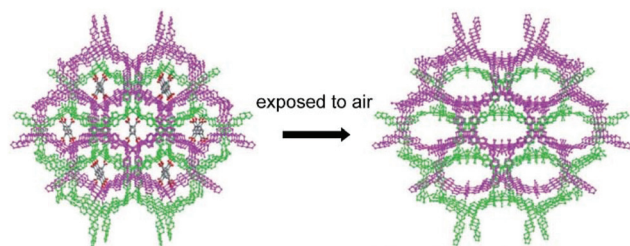


Fig. 24 Transformation from the (3,8)-connected self-penetrating network **46** to the (3,6)-connected two-fold interpenetrated network **46'**. Reprinted with permission from ref. 73. Copyright (2013) John Wiley and Sons.

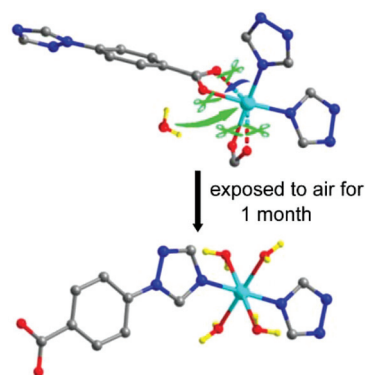


Fig. 25 Rearrangement of coordination interactions around $\text{Cu}(\text{II})$ ion in the SCSC transformation from **47** (top) to **47'** (bottom) upon thermodynamic hydration. Reprinted with permission from ref. 74. Copyright (2014) American Chemical Society.

ligands to construct 3D **dia** networks, which are further entangled with each other to form a 4-fold interpenetrated framework. Upon thermodynamic hydration, the metal centers in **47** suffered a slow attack by water molecules. After exposure to air for about one month, a visible SCSC transformation occurred, and the mononuclear complex $[\text{Cu}(\text{tba})_2(\text{H}_2\text{O})_4]$ (**47'**) was obtained (Fig. 25). Single-crystal XRD data revealed that each $\text{Cu}(\text{II})$ cluster in **47'** is coordinated by two tba ligands and four water molecules, indicating the destruction of all Cu-carboxylate interactions and meanwhile, the formation of four Cu-water coordination bonds. All ligands around the metal clusters rearrange themselves into a trans orientation to suit the new structure of **47'**. It is worth mentioning that crystals of **47** have a high adsorption selectivity of CO_2 over a variety of other gases.

The examples discussed above show that SCSC transformations can bring a variety of changes to the original structures, such as variations in the metal coordination environment, changes in the structure dimensionality and changes in the network entanglement characteristics. These transformations can even provide a means to obtain new molecules that are otherwise difficult or impossible to synthesize by traditional methods. As for complexes **28**, **29** and **30**, there are chemical bonds that break at SBUs or at linkers, but there are no big changes to the entire structure. This kind of transformation happens within the partial sites of the framework. In contrast, changing the dimensionality or changing the entanglement characteristics of one framework is a drastic process and needs more energy. Old chemical bonds need to be broken and the vacant coordination sites at the metal centers created by the removal of ligands are often found to be reestablished by free donors of the neighboring ligands when different skeletons come close to each other. In this way, new chemical bonds are formed, and then the structure dimensionality increases or rearrangement of the whole net is accomplished. In other words, if the dimensionality is increased or the entanglement characteristics of one framework is changed, it is always accompanied by the formation of new chemical bonds. This analysis can be applied to complexes **31–47**.

4. SCSC transformation induced by temperature change

All of the structural transformations mentioned in part 3 are triggered by the loss/uptake of solvent vapor, which is mainly achieved by an increase in temperature. Temperature is one of the most common factors to influence the final structure of MOF materials, and solvent molecule removal by heating is one of the most direct methods to prompt these various solid-state transformations. However, sometimes a change in the entire framework can directly result from temperature variation, with no solvent vapor participation. In the following section, we will discuss SCSC transformations taking place in such a manner, triggered merely by temperature increases or decreases, and involving bond breakage, bond formation and lattice motion.

In 2012, Ovcharenko *et al.* reported a reversible SCSC transformation by means of polymerization and depolymerization initiated by a temperature change.⁷⁵ In this case, molecules experienced considerable displacements in the single-crystal state, retaining the crystal integrity. Complex $[[\text{Cu}(\text{hfac})_2]_3(\mu\text{-O},\text{N-L}^5)_2][\text{Cu}(\text{hfac})_2(\text{O-L}^5)_2]$ (**48**, hfac = hexafluoroacetylacetonate, L^5 = nitronyl nitroxide 2-(1-ethyl-3-methyl-1*H*-pyrazol-4-yl)-4,4,5,5-tetramethyl-4,5-dihydro-1*H*-imidazole-3-oxide-1-oxyl) has two components, a tri-nuclear molecule and a mononuclear molecule. In the tri-nuclear part, Cu atoms are coordinated by four oxygen atoms in the square and one nitrogen atom at the terminal position, adopting a five-coordinated square pyramid geometry. Meanwhile, the mononuclear molecule has a free nitrogen atom in the ligand of L^5 . When complex **48** was cooled below 225 K, the distance between the Cu atom of the tri-nuclear molecule and the N atom of L^5 decreased to 2.460 Å. A new Cu–N bond was generated and the coordination geometry of Cu(II) changed from square-pyramidal mode to octahedral. Thus, the molecular structure of **48** transformed to a 1D polymer chain structure of $[\text{Cu}(\text{hfac})_2(\mu\text{-O},\text{N-L}^5)]_\infty$ (**48'**), as illustrated in Fig. 26. When the low-temperature

phase was heated to above 270 K, the polymer chain structure decomposed and complex **48'** again transformed back to a molecular pair complex. This structural conversion was accompanied by a magnetic anomaly caused by the modulation of the odd electrons of the Cu(II) ion and nitroxide, resulting in a reversible transition from antiferromagnetic to ferromagnetic coupling.

Other similar transformations were reported by Kaskel,^{76,77} Dong,⁷⁸ Tzeng,⁷⁹ Fan,⁸⁰ Srivastava⁸¹ and Julve *et al.*⁸²

5. SCSC transformation induced by mechanical force

5.1 Mechano-chemical grinding

Mechano-chemical grinding is one of the most common ways to apply mechanical force, and is widely used in the synthesis of many organic, inorganic, organometallic and metal–organic hybrid materials. The application of mechanical force results in various types of structural transformations because it can cause diverse movements of atoms at the micro level, such as the loss or uptake of solvent molecules, exchange of coordinated ions and pedal-like motion of molecular fragments. Furthermore, grinding can increase the solid-state reaction activity by facilitating movement of molecules to align themselves in parallel mode, as required for photodimerization reactions, examples of which have been thoroughly discussed in part 2. Apart from a few SCSC examples, transformations induced by mechano-chemical grinding usually cannot be investigated directly by single-crystal X-ray crystallography. However, at the microcrystalline scale the crystalline form is maintained, with larger crystals simply being broken down into tiny ones. In these situations, the PXRD patterns of the bulk sample are often compared with simulated ones from the single-crystal data obtained from other routes, and structural analysis directly obtained using PXRD diffraction data is also widely performed.

Schmidt's topochemical criteria for photochemical [2 + 2] cycloadditions have been leading the way in organic photochemistry for the past few years. In some systems, this kind of reaction can be effectively accelerated by mechanical grinding. In 2008, Vittal *et al.* reported a hydrogen-bonded coordination complex, $[\text{Zn}(\text{bpe})_2(\text{H}_2\text{O})_4](\text{NO}_3)_2 \cdot 8/3\text{H}_2\text{O} \cdot 2/3\text{bpe}$ (**49**), which exhibited a mechano-chemical force-promoted structural transformation.⁸³ When single crystals of **49** were subjected to UV light for 25 h, 46% photochemical conversion was observed. However, when the single crystals were ground to a powder for 5 min and subjected to UV irradiation for 4 h, 88% conversion of C=C bonds to cyclobutane rings was observed. This kind of conversion increase has been observed in many [2 + 2] cycloaddition reactions, such as the situations for complexes **17** and **18**. In some cases, the conversion cannot reach 100% unless the crystals are ground. Grinding increases the surface area, and the reactivity is greatly increased when a sample with a larger surface is exposed to UV irradiation. Meanwhile, grinding accelerates the pedal motion of olefins to

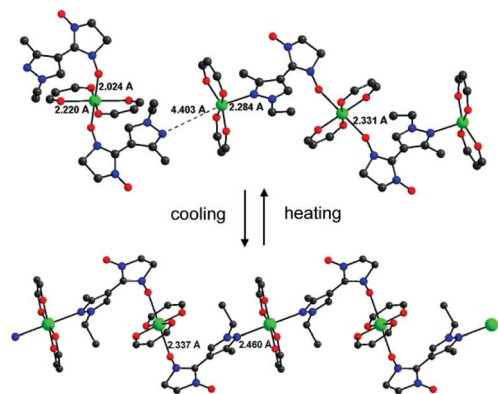


Fig. 26 Transformation from the molecular structure of **48** to the 1D polymer chain structure of **48'**. Reprinted with permission from ref. 75. Copyright (2012) American Chemical Society.

parallel alignment, leading to better interactions between active sites so as to achieve a higher reaction rate and a higher conversion. In complex **49**, there are six olefins in a row that satisfy Schmidt distance criterion, of which four lie in a criss-cross conformation and two have parallel orientation. Grinding the single crystals into a powder accelerates the parallel alignment as well as the motion of free bpe in the solid. So, the powdered sample undergoes quantitative conversion with rctt-tpcb as a major product. Thus, mechano-chemical grinding not only can increase the surface area of the reactor, but can also accelerate the molecular pedal motion, both of which will increase the activity of the solid-state reaction. This phenomenon has been witnessed in a lot of UV-induced photodimerization reactions.

In 2011, Sun *et al.* reported a complex, $[\text{Cu}(\text{NH}_3)_3(\text{L}^6)] \cdot (\text{H}_2\text{O})_{0.66}$ (**50**, $\text{H}_2\text{L}^6 = 2,2'-(1,2\text{-phenylenebis(methylene))bis(sulfanediyl)-dibenzoic acid}$), which could be dimerized to form a binuclear complex *via* thermal treatment or dry grinding.⁸⁴ In the structure of **50**, the copper ion adopts a square-planar coordinated geometry with one oxygen atom from ligand L^6 and three ammonia molecules. The hydrogen-bonding interactions connect the mononuclear copper complexes into double-helical chains, which are further connected to one another to generate a 1D tube. Every two monomers in **50** adopt a head-to-tail arrangement. The distance between Cu and O in the neighboring monomer is 3.796 Å, which satisfies the distance for the formation of new coordination bonds. Based on the above-mentioned analysis, a temperature increase was carried out first. After heating at 176 °C for 15 min, a new crystal **50'** was generated. Single-crystal X-ray diffraction revealed that the most obvious change was the dimerization from monomer **50** to a 30-membered metallo-macrocycle **50'**, with a coordination geometry change in the copper ion from square-planar to square-pyramidal. Subsequently, this structural transformation was achieved by solid-state grinding. Ball milling of monomer **50** was performed in a QM-3B shaker mill, which was accompanied by a color change from blue to light gray-blue, which was consistent with the phenomenon induced by heating. Powder X-ray diffraction results finally proved the accomplishment of the total transformation from **50** to **50'** (Fig. 27). This transformation from **50** to **50'** represents the first dimerization of a metal complex through a mechano-chemical reaction.

It is well known that using KBr pellets prepared by mechanical grinding or ball milling is the routine pre-treatment method for infrared analysis. A few supramolecular structural transformations have been accidentally achieved while making KBr pellets. Carboxylate ligands can be easily replaced by bromide ions, so a number of complexes have been formed *via* ion exchange reactions with KBr in the solid state. One example of this type of ligand exchange was reported by Stephens and Vittal *et al.* in 2012.⁸⁵ Two 1D polymers $[\text{Zn}_2(\mu\text{-bpe})_2(\mu\text{-CH}_3\text{CO}_2)_2(\text{CF}_3\text{CO}_2)_2]$ (**51**) and $[\text{Cd}(\mu\text{-bpe})(\text{CH}_3\text{CO}_2)_2(\text{H}_2\text{O})]$ (**52**) both underwent subsequent transformations to generate bromide-bridged polymers upon grinding with KBr. When **51** was ground with solid KBr in a 1 : 2 molar

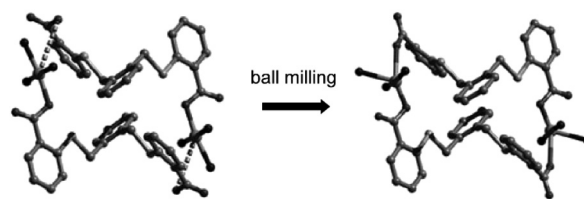


Fig. 27 The transformation from **50** to **50'** through solid-state reaction under grinding. Reprinted with permission from ref. 84. Copyright (2011) John Wiley and Sons.

ratio for 20 min, the PXRD pattern implied that a new product $[\text{Zn}(\mu\text{-bpe})(\text{Br})_2]$ **51'** was obtained (Fig. 28), as evidenced by the complete disappearance of **51** peaks. Crystals of **51'** could also be constructed *via* a solvothermal method. Single-crystal X-ray analysis revealed that there is a 1D zigzag chain in **51'** consisting of tetrahedral Zn(II) ions bridged by bpe ligands and two terminal bromide ions, indicating that the acetate was replaced by bromide ligands. The visible accurate crystal structure exactly confirms this solid-state transformation induced by mechano-chemical grinding. Similarly, complex **52** changed into a 2D sheet-like coordination polymer $[\text{Cd}(\mu\text{-bpe})(\mu\text{-Br})_2]$ (**52'**) when the acetate ligands were replaced by bridging bromide ligands.

Ligand exchange by another two ions was reported by Morsali *et al.*⁸⁶ The 3D Pb(II) coordination polymer $[\text{Pb}(\text{L}^7)(\mu_2\text{-Cl})(\text{H}_2\text{O})]_n$ (**53**, $\text{HL}^7 = 1H\text{-}1,2,4\text{-triazole-}3\text{-carboxylic acid}$) can undergo irreversible SCSC transformations to $[\text{Pb}(\text{L}^7)(\mu_2\text{-Br})(\text{H}_2\text{O})]_n$ (**53'**) and $[\text{Pb}(\text{L}^7)(\mu_{1,1}\text{-NCS})(\text{H}_2\text{O})]_n$ (**53''**) *via* solid-state mechano-chemical reactions. Through grinding with solid KBr and KSCN, complex **53** transformed into **53'** and **53''**, whose chloride ligands were replaced by bromide and thiocyanate, respectively. The resulting products, **53'** and **53''**, were confirmed by powder X-ray diffraction. The patterns obtained were well matched to the patterns calculated from the single-crystal

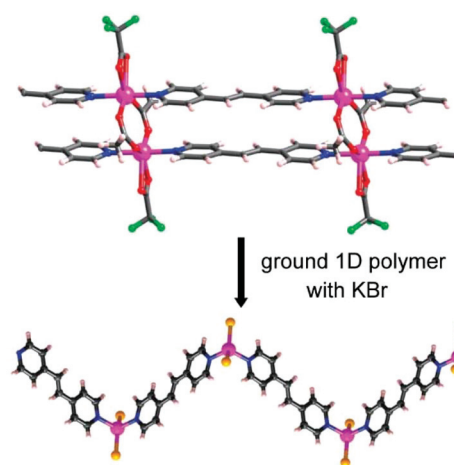


Fig. 28 Solid-state transformation from the 1D ladder coordination polymer **51** to the zigzag coordination polymer **51'**. Reprinted with permission from ref. 85. Copyright (2012) Royal Society of Chemistry.

X-ray data of **53'** and **53''**, which further confirmed this transformation. IR spectra of these complexes demonstrated the existence of the corresponding anions, further verifying these irreversible anion-replacements. Another two similar anion-exchange processes were found for the complexes $[\text{Pb}(\text{L}^8)(\mu_2\text{-Br})(\text{H}_2\text{O})]_n$ (**54**, $\text{HL}^8 = 1H\text{-}1,2,4\text{-triazole-}3\text{-carboxylic acid}$)⁸⁷ and $[\text{Pb}(4\text{-bpdh})(\mu\text{-NCS})_2]_n$ (**55**, $4\text{-bpdh} = 2,5\text{-bis}(4\text{-pyridyl})\text{-}3,4\text{-diaz-}2,4\text{-hexadiene}$).⁸⁸ Different from the above-mentioned unidirectional transformations, **54** and **55** underwent this type of anion-replacement reversibly.

In 2013, Vittal *et al.* reported another kind of solid-state transformation in which the sheet structure of the complex rearranged itself into a ladder polymer when the desolvated single crystals were ground into a powder.⁸⁹ This structural rearrangement was demonstrated by the usage of photochemical reactions to follow the formation of thermodynamically stable ladder structures.

5.2 Partial mechanical force

Anisotropic forces at the bulk scale normally break the integrity of a single crystal. Therefore, crystals obtained from solid-state transformations induced by mechano-chemical grinding are always too small to be determined by single-crystal X-ray crystallography. However, if the structural transformation is triggered by a small pit on the crystal surface by needle pricking, the integrity of the single crystal can be completely maintained. This phenomenon has been observed in a few coordination supramolecular crystals.

In 2013, Ito *et al.* reported the first example of a SCSC transformation triggered by mechanical force in molecular crystals. Through controlling the rate of crystallization in a mixed solvent solution, two different phases of crystal **56**, **I_b** phase and **II_y** phase, were obtained (Fig. 29).⁹⁰ In **I_b**, there is a dihedral angle of 71.6° between the plane of the phenyl ligand on the gold atoms and the plane of the isocyanide phenyl moiety. In contrast, **II_y** exhibits a significantly different structure. Molecules in **II_y** adopt a nearly flat conformation, and the dihedral angle of those two portions described above is only 3.1°. Blue photoluminescence was observed from **I_b** crystals, while the **II_y** crystals exhibited a strong yellow emission. The emission quantum yields, emission lifetimes and the excitation spectra of these two phases are all different. By first mechanically grinding and then ball-milling **I_b**, the powder form of **II_y(ground I_b)** was afforded, whose data was identical to the crystalline **II_y** in terms of photoluminescence and the powder XRD analysis. Further, a special external mechanical stimulus, applied using a needle, was exerted on this system. The surface of a crystal of **I_b** was pitted using a small needle. A yellow luminescent spot was observed immediately at the location of the small pit. This luminescence color changed and extended to the entire crystal after 9 h at room temperature. This phase transformation happened like dominoes, in which a mechanical stimulus triggers a phase change in the entire assembly. This transformation could be reproduced by only pure contact of **II_y** and **I_b**. Single-crystal X-ray analysis revealed that the crystal structure of **II_ysc** obtained *via* SCSC

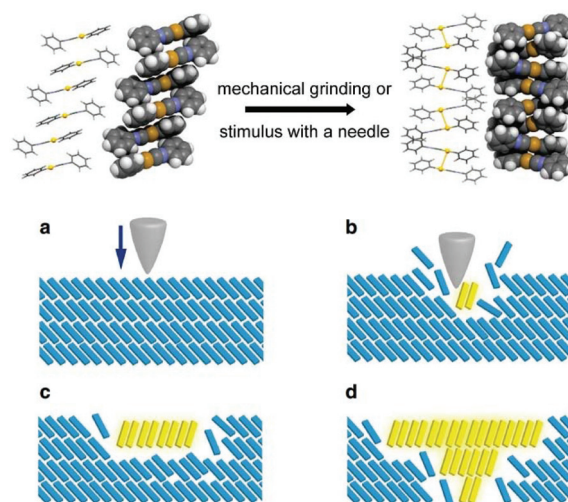


Fig. 29 Top: SCSC transformation triggered by mechanical force in **56**. Bottom: Proposed mechanism for the mechanical stimulus-triggered phase transformation. (a) Mechanical stimulation of the metastable **I_b** phase (blue rectangles). (b) Generation of the **II_y** phase. (c and d) The thermodynamically stable **II_y** phase extends by absorbing molecules from the metastable **I_b** phase. Reprinted with permission from ref. 90. Copyright (2013) Nature Publishing Group.

transformation is identical to that of **II_y** crystallized from the solution phase, providing a molecular-level identification of this phase transformation. The **I_b** phase could change into the **II_y** phase, but the inverse process could not be achieved using mechanical force, only if dissolution and recrystallization was carried out. It also proves the thermodynamic stability of the **II_y** phase at the same time. Other similar molecular reorientations induced by mechanical force have also been reported by Ito *et al.*⁹¹

In 2014, Tao *et al.* reported a new polymorph cocrystal, 7,7,8,8-tetracyanoquinodimethane-*p*-bis(8-hydroxyquinolino) copper(II) (**57**, Form II), whose dimensions could change drastically under mechanical stimulation.⁹² Crystals of **57** obtained by a routine method at room temperature were defined as Form II. Once the (001) face of Form II was pricked by a metal needle, a remarkable dimensionality change was observed. Complete transformation without crystal breakage gave birth to a new form, Form I, and the whole transition took only a few seconds. The crystal face changed from Form II to Form I, resulting in an apparent change of the crystal to half of its original thickness and double its original length (Fig. 30). This SCSC transformation indicated that Form II is a metastable state relative to Form I and the differences between Form II and Form I in layer stacking patterns are responsible for this SCSC process.

6. Summary and outlook

In this review, we have presented recent efforts to enhance the understanding of solid-state reactivity and dynamic structural

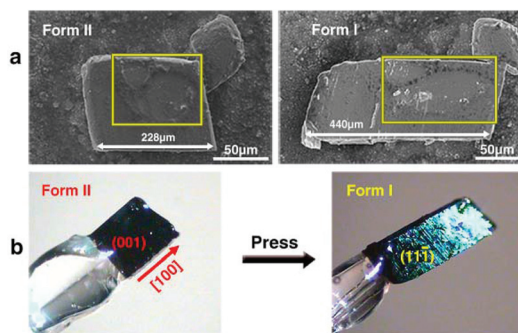


Fig. 30 (a) Scanning electron microscopy images of crystal 57 before and after the phase transition. (b) Face-indexing graphics of the same piece of crystal before and after the phase transition. Reprinted with permission from ref. 92. Copyright (2014) American Chemical Society.

transformations of coordination polymers in SCSC mode. All of the transformations discussed above are entirely liquid-free (both the reactant and product are in the solid phase), and we have strictly excluded those involving liquids, in which the transformation occurs in a recrystallization manner. All of the transformations involve major structural changes rather than twisting phenomena, with breakage or formation of at least one type of chemical bond. In an attempt to better establish the relationship between external factors and structural transformations for these crystals, different exogenous stimuli, including UV light, loss/uptake of solvent vapor, temperature change, mechanical force and synergic effects, have each been discussed.

The coordination bonds of transition metals are relatively weak, so bonds in or around the metal nodes are the most fragile sites in MOFs and coordination polymers. This is the essential reason for the thermal and chemical instability of these materials. However, this is also the reason why these metal sites are the most reactive. In reactions involving solid-state transformations stimulated by heating or mechano-chemical grinding, metal sites are at the forefront of the whole structure. Breakage or formation of the coordination bonds around transition metal ions results in changes in the coordination geometries, leading to a variety of possible changes in the network's entanglement characteristics and structure dimensionality. On the other hand, upon exposure to UV or heating, organic linkers can also undergo appropriate transformations, such as ligand polymerization and ligand modification, and this phenomenon usually happens in $[2 + 2]$ photochemical reactions.

Up to now, aside from the most widely-used technique of single-crystal X-ray diffraction, powder diffraction methods are becoming the dominant structural tool to follow these solid-state structural transformations. With the help of theoretical calculation methods and modern structure determination tools, detailed structures of tiny crystals can be obtained and many systems involving tiny crystalline transformations can be routinely studied.

However, the investigation of SCSC transformations is still in its infancy. Research into UV-induced $[2 + 2]$ photochemical reactions is the most mature field among these transformations. For the other ways, although many solvent-induced and mechanical force-induced reactions have been reported, the mechanisms behind most transformations still remain unclear and out of control. One system may be able to undergo a certain class of transformation, while similar structures may not exhibit a structural transfer belonging to this category. All studies so far have been at the test stage, and have not involved a controllable process with specific targets.

In conclusion, through the process of SCSC transformations, we have obtained some new coordination supramolecular systems and new organic ligands, which cannot be obtained using routine synthetic methods, as well as a deep understanding of the formation and breakage of chemical bonds. More fascinatingly, these new complexes obtained from structural transformations have peculiar physicochemical properties in adsorption, magnetism, luminescence, chirality and catalysis. With rapid progress in research, we suppose that SCSC transformations will become an auxiliary method, to be used before or after other chemical synthesis processes, that will aid the design and synthesis of more functional materials.

Conflicts of interest

There are no conflicts to declare.

Acknowledgements

This work was financially supported by the National Natural Science Foundation of China (No. 21701016, 21622104 and 21471080), Priority Academic Program Development of Jiangsu Higher Education Institutions and the Foundation of Jiangsu Collaborative Innovation Center of Biomedical Functional Materials.

References

- 1 G. Maurin, C. Serre, A. Cooper and G. Ferey, *Chem. Soc. Rev.*, 2017, **46**, 3104.
- 2 A. H. Chughtai, N. Ahmad, H. A. Younus, A. Laypkov and F. Verpoort, *Chem. Soc. Rev.*, 2015, **44**, 6804.
- 3 X. Lian, Y. Fang, E. Joseph, Q. Wang, J. Li, S. Banerjee, C. Lollar, X. Wang and H.-C. Zhou, *Chem. Soc. Rev.*, 2017, **46**, 3386.
- 4 M. Rubio-Martinez, C. Avci-Camur, A. W. Thornton, I. Imaz, D. Maspoth and M. R. Hill, *Chem. Soc. Rev.*, 2017, **46**, 3453.
- 5 Y.-J. Tang, M.-R. Gao, C.-H. Liu, S.-L. Li, H.-L. Jiang, Y.-Q. Lan, M. Han and S.-H. Yu, *Angew. Chem., Int. Ed.*, 2015, **54**, 12928.

- 6 J.-S. Li, Y. Wang, C.-H. Liu, S.-L. Li, Y.-G. Wang, L.-Z. Dong, Z.-H. Dai, Y.-F. Li and Y.-Q. Lan, *Nat. Commun.*, 2016, **7**, 11204.
- 7 W. P. Lustig, S. Mukherjee, N. D. Rudd, A. V. Desai, J. Li and S. K. Ghosh, *Chem. Soc. Rev.*, 2017, **46**, 3242.
- 8 J. Liu and C. Woll, *Chem. Soc. Rev.*, 2017, **46**, 5730.
- 9 (a) S. Furukawa, J. Reboul, S. Diring, K. Sumida and S. Kitagawa, *Chem. Soc. Rev.*, 2014, **43**, 5700; (b) J.-P. Zhang and X.-M. Chen, *J. Am. Chem. Soc.*, 2008, **130**, 6010; (c) J.-P. Zhang and X.-M. Chen, *J. Am. Chem. Soc.*, 2009, **131**, 5516; (d) P.-Q. Liao, D.-D. Zhou, A.-X. Zhu, L. Jiang, R.-B. Lin, J.-P. Zhang and X.-M. Chen, *J. Am. Chem. Soc.*, 2012, **134**, 17380.
- 10 (a) Z.-J. Lin, J. Lu, M. Hong and R. Cao, *Chem. Soc. Rev.*, 2014, **43**, 5867; (b) Y.-S. Wei, M. Zhang, P.-Q. Liao, R.-B. Lin, T.-Y. Li, G. Shao, J.-P. Zhang and X.-M. Chen, *Nat. Commun.*, 2015, **6**, 8348; (c) P.-Q. Liao, A.-X. Zhu, W.-X. Zhang, J.-P. Zhang and X.-M. Chen, *Nat. Commun.*, 2015, **6**, 6350.
- 11 S. M. J. Rogge, A. Bavykina, J. Hajek, H. Garcia, A. I. Olivoso-Suarez, A. Sepulveda-Escribano, A. Vimont, G. Clet, P. Bazin, F. Kapteijn, M. Daturi, E. V. Ramos-Fernandez, F. X. Llabres i Xamena, V. Van Speybroeck and J. Gascon, *Chem. Soc. Rev.*, 2017, **46**, 3134.
- 12 K. Adil, Y. Belmabkhout, R. S. Pillai, A. Cadiau, P. M. Bhatt, A. H. Assen, G. Maurin and M. Eddaoudi, *Chem. Soc. Rev.*, 2017, **46**, 3402.
- 13 H. Assi, G. Mouchaham, N. Steunou, T. Devic and C. Serre, *Chem. Soc. Rev.*, 2017, **46**, 3431.
- 14 V. V. Boldyrev, *Reactivity of Solids: Past, Present and Future*, Blackwell Science, Cambridge, 1996.
- 15 F. Toda, *Organic Solid State Reactions*, Springer, The Netherlands, 2005.
- 16 (a) W.-W. He, S.-L. Li, H.-Y. Zang, G.-S. Yang, S.-R. Zhang, Z.-M. Su and Y.-Q. Lan, *Coord. Chem. Rev.*, 2014, **279**, 141; (b) Y.-S. Wei, K.-J. Chen, P.-Q. Liao, B.-Y. Zhu, R.-B. Lin, H.-L. Zhou, B.-Y. Wang, W. Xue, J.-P. Zhang and X.-M. Chen, *Chem. Sci.*, 2013, **4**, 1539; (c) H.-L. Zhou, R.-B. Lin, C.-T. He, Y.-B. Zhang, N. Feng, Q. Wang, F. Deng, J.-P. Zhang and X.-M. Chen, *Nat. Commun.*, 2013, **4**, 2534; (d) H.-L. Zhou, Y.-B. Zhang, J.-P. Zhang and X.-M. Chen, *Nat. Commun.*, 2015, **6**, 6917.
- 17 D.-Y. Du, J.-S. Qin, S.-L. Li, Z.-M. Su and Y.-Q. Lan, *Chem. Soc. Rev.*, 2014, **43**, 4615.
- 18 G. M. J. Schmidt, *Pure Appl. Chem.*, 1971, **27**, 647–678.
- 19 J.-K. Sun, W. Li, C. Chen, C.-X. Ren, D.-M. Pan and J. Zhang, *Angew. Chem., Int. Ed.*, 2013, **52**, 6653.
- 20 D. Liu, H.-F. Wang, B. F. Abrahams and J.-P. Lang, *Chem. Commun.*, 2014, **50**, 3173.
- 21 G. K. Kole, A. M. P. Peedikakkal, B. M. F. Toh and J. J. Vittal, *Chem. – Eur. J.*, 2013, **19**, 3962.
- 22 C.-P. Li, J. Chen, C.-S. Liu and M. Du, *Chem. Commun.*, 2015, **51**, 2768.
- 23 A. Chaudhary, A. Mohammad and S. M. Mobin, *Cryst. Growth Des.*, 2017, **17**, 2893.
- 24 (a) G. K. Kole and J. J. Vittal, *Chem. Soc. Rev.*, 2013, **42**, 1755; (b) J.-P. Zhang, P.-Q. Liao, H.-L. Zhou, R.-B. Lin and X.-M. Chen, *Chem. Soc. Rev.*, 2014, **43**, 5789; (c) J.-P. Zhang, H.-L. Zhou, D.-D. Zhou, P.-Q. Liao and X.-M. Chen, *Natl. Sci. Rev.*, 2017, DOI: 10.1093/nsr/nwx127.
- 25 C.-P. Li and M. Du, *Chem. Commun.*, 2011, **47**, 5958.
- 26 W. L. Leong and J. J. Vittal, *Chem. Rev.*, 2011, **111**, 688.
- 27 R. Medishetty, I.-H. Park, S. S. Lee and J. J. Vittal, *Chem. Commun.*, 2016, **52**, 3989.
- 28 R. Medishetty, R. Tandiana, J. Wu, Z. Bai, Y. Du and J. J. Vittal, *Chem. – Eur. J.*, 2015, **21**, 11948.
- 29 N. L. Toh, M. Nagarathinam and J. J. Vittal, *Angew. Chem., Int. Ed.*, 2005, **44**, 2237.
- 30 D. Liu, N.-Y. Li and J.-P. Lang, *Dalton Trans.*, 2011, **40**, 2170.
- 31 A. Chanthapally, G. K. Kole, K. Qian, G. K. Tan, S. Gao and J. J. Vittal, *Chem. – Eur. J.*, 2012, **18**, 7869.
- 32 S.-Y. Yang, X.-L. Deng, R.-F. Jin, P. Naumov, M. K. Panda, R.-B. Huang, L.-S. Zheng and B. K. Teo, *J. Am. Chem. Soc.*, 2014, **136**, 558.
- 33 M. H. Mir, L. L. Koh, G. K. Tan and J. J. Vittal, *Angew. Chem., Int. Ed.*, 2010, **49**, 390.
- 34 D. Liu, Z.-G. Ren, H.-X. Li, J.-P. Lang, N.-Y. Li and B. F. Abrahams, *Angew. Chem., Int. Ed.*, 2010, **49**, 4767.
- 35 I.-H. Park, A. Chanthapally, H.-H. Lee, H. S. Quah, S. S. Lee and J. J. Vittal, *Chem. Commun.*, 2014, **50**, 3665.
- 36 W.-J. Gong, Z.-G. Ren, H.-X. Li, J.-G. Zhang and J.-P. Lang, *Cryst. Growth Des.*, 2017, **17**, 870.
- 37 Q. Chu, D. C. Swenson and L. R. MacGillivray, *Angew. Chem., Int. Ed.*, 2005, **44**, 3569.
- 38 S. Dutta, D.-K. Bucar, E. Elacqua and L. R. MacGillivray, *Chem. Commun.*, 2013, **49**, 1064.
- 39 K. M. Hutchins, T. P. Rupasinghe, L. R. Ditzler, D. C. Swenson, J. R. G. Sander, J. Baltrusaitis, A. V. Tivanski and L. R. MacGillivray, *J. Am. Chem. Soc.*, 2014, **136**, 6778.
- 40 R. Medishetty, T. T. S. Yap, L. L. Koh and J. J. Vittal, *Chem. Commun.*, 2013, **49**, 9567.
- 41 A. M. P. Peedikakkal and J. J. Vittal, *Inorg. Chem.*, 2010, **49**, 10.
- 42 D. Liu, J.-P. Lang and B. F. Abrahams, *Chem. Commun.*, 2013, **49**, 2682.
- 43 Y.-C. Ou, D.-S. Zhi, W.-T. Liu, Z.-P. Ni and M.-L. Tong, *Chem. – Eur. J.*, 2012, **18**, 7357.
- 44 R. Medishetty, L. L. Koh, G. K. Kole and J. J. Vittal, *Angew. Chem., Int. Ed.*, 2011, **50**, 10949.
- 45 R. Medishetty, R. Tandiana, L. L. Koh and J. J. Vittal, *Chem. – Eur. J.*, 2014, **20**, 1231.
- 46 M.-H. Xie, X.-L. Yang and C.-D. Wu, *Chem. – Eur. J.*, 2011, **17**, 11424.
- 47 Z. Su, M. Chen, T.-a. Okamura, M.-S. Chen, S.-S. Chen and W.-Y. Sun, *Inorg. Chem.*, 2011, **50**, 985.
- 48 Q. Chen, J.-B. Lin, W. Xue, M.-H. Zeng and X.-M. Chen, *Inorg. Chem.*, 2011, **50**, 2321.
- 49 A. K. Chaudhari, S. S. Nagarkar, B. Joarder, S. Mukherjee and S. K. Ghosh, *Inorg. Chem.*, 2013, **52**, 12784.

- 50 Z. Niu, J.-G. Ma, W. Shi and P. Cheng, *Chem. Commun.*, 2014, **50**, 1839.
- 51 X.-M. Lin, T.-T. Li, Y.-W. Wang, L. Zhang and C.-Y. Su, *Chem. – Asian J.*, 2012, **7**, 2796.
- 52 Y. Yu, X.-M. Zhang, J.-P. Ma, Q.-K. Liu, P. Wang and Y.-B. Dong, *Chem. Commun.*, 2014, **50**, 1444.
- 53 J. Girard and K. Fromm, *CrystEngComm*, 2012, **14**, 6487.
- 54 M. K. Sharma and P. K. Bharadwaj, *Inorg. Chem.*, 2011, **50**, 1889.
- 55 X. Liu, P. Cen, H. Li, H. Ke, S. Zhang, Q. Wei, G. Xie, S. Chen and S. Gao, *Inorg. Chem.*, 2014, **53**, 8088.
- 56 F. Sun, Z. Yin, Q.-Q. Wang, D. Sun, M.-H. Zeng and M. Kurmoo, *Angew. Chem., Int. Ed.*, 2013, **52**, 4538.
- 57 H. H. M. Yeung, M. Kosa, J. M. Griffin, C. P. Grey, D. T. Major and A. K. Cheetham, *Chem. Commun.*, 2014, **50**, 13292.
- 58 J.-P. Zhang, Y.-Y. Lin, W.-X. Zhang and X.-M. Chen, *J. Am. Chem. Soc.*, 2005, **127**, 14162.
- 59 X.-D. Chen, X.-H. Zhao, M. Chen and M. Du, *Chem. – Eur. J.*, 2009, **15**, 12974.
- 60 H. Aggarwal, P. M. Bhatt, C. X. Bezuidenhout and L. J. Barbour, *J. Am. Chem. Soc.*, 2014, **136**, 3776.
- 61 P. Shen, W.-W. He, D.-Y. Du, H.-L. Jiang, S.-L. Li, Z.-L. Lang, Z.-M. Su, Q. Fu and Y.-Q. Lan, *Chem. Sci.*, 2014, **5**, 1368.
- 62 D.-D. Zhou, Z.-J. Liu, C.-T. He, P.-Q. Liao, H.-L. Zhou, Z.-S. Zhong, R.-B. Lin, W.-X. Zhang, J.-P. Zhang and X.-M. Chen, *Chem. Commun.*, 2015, **51**, 12665.
- 63 (a) S. K. Ghosh, J.-P. Zhang and S. Kitagawa, *Angew. Chem., Int. Ed.*, 2007, **46**, 7965; (b) W. Kaneko, M. Ohba and S. Kitagawa, *J. Am. Chem. Soc.*, 2007, **129**, 13706; (c) K. D. Demadis, M. Papadaki, M. A. G. Aranda, A. Cabeza, P. Olivera-Pastor and Y. Sanakis, *Cryst. Growth Des.*, 2010, **10**, 357.
- 64 J. Olchowka, C. Falaise, C. Volkringer, N. Henry and T. Loiseau, *Chem. – Eur. J.*, 2013, **19**, 2012.
- 65 Y.-J. Zhang, T. Liu, S. Kanegawa and O. Sato, *J. Am. Chem. Soc.*, 2010, **132**, 912.
- 66 (a) X.-N. Cheng, W.-X. Zhang and X.-M. Chen, *J. Am. Chem. Soc.*, 2007, **129**, 15738; (b) E. Coronado and G. Minguez Espallargas, *Chem. Soc. Rev.*, 2013, **42**, 1525.
- 67 Q.-Q. Li, C.-Y. Ren, Y.-Y. Huang, J.-L. Li, P. Liu, B. Liu, Y. Liu and Y.-Y. Wang, *Chem. – Eur. J.*, 2015, **21**, 4703.
- 68 S.-J. Liu, C. Cao, S.-L. Yao, T.-F. Zheng, Z.-X. Wang, C. Liu, J.-S. Liao, J.-L. Chen, Y.-W. Li and H.-R. Wen, *Dalton Trans.*, 2017, **46**, 64.
- 69 Z.-S. Cai, S.-S. Bao, X.-Z. Wang, Z. Hu and L.-M. Zheng, *Inorg. Chem.*, 2016, **55**, 3706.
- 70 B.-C. Tzeng, T.-Y. Chang and H.-S. Sheu, *Chem. – Eur. J.*, 2010, **16**, 9990.
- 71 B.-C. Tzeng, T.-Y. Chang, S.-L. Wei and H.-S. Sheu, *Chem. – Eur. J.*, 2012, **18**, 5105.
- 72 S. B. Choi, H. Furukawa, H. J. Nam, D.-Y. Jung, Y. H. Jhon, A. Walton, D. Book, M. O'Keeffe, O. M. Yaghi and J. Kim, *Angew. Chem., Int. Ed.*, 2012, **51**, 8791.
- 73 Q. Chen, Z. Chang, W.-C. Song, H. Song, H.-B. Song, T.-L. Hu and X.-H. Bu, *Angew. Chem., Int. Ed.*, 2013, **52**, 11550.
- 74 M. Du, C.-P. Li, M. Chen, Z.-W. Ge, X. Wang, L. Wang and C.-S. Liu, *J. Am. Chem. Soc.*, 2014, **136**, 10906.
- 75 V. I. Ovcharenko, S. V. Fokin, E. T. Kostina, G. V. Romanenko, A. S. Bogomyakov and E. V. Tretyakov, *Inorg. Chem.*, 2012, **51**, 12188.
- 76 K. Gedrich, I. Senkovska, I. A. Baburin, U. Mueller, O. Trapp and S. Kaskel, *Inorg. Chem.*, 2010, **49**, 4440.
- 77 I. M. Hauptvogel, R. Biedermann, N. Klein, I. Senkovska, A. Cadiau, D. Wallacher, R. Feyerherm and S. Kaskel, *Inorg. Chem.*, 2011, **50**, 8367.
- 78 J.-P. Ma, S.-C. Liu, C.-W. Zhao, X.-M. Zhang, C.-Z. Sun and Y.-B. Dong, *CrystEngComm*, 2014, **16**, 304.
- 79 B.-C. Tzeng, M. Banik, T. Selvam and G.-H. Lee, *Cryst. Growth Des.*, 2013, **13**, 4245.
- 80 S. Gao, R.-Q. Fan, L.-S. Qiang, P. Wang, S. Chen, X.-M. Wang and Y.-L. Yang, *CrystEngComm*, 2014, **16**, 1113.
- 81 S. M. Mobin, A. K. Srivastava, P. Mathur and G. K. Lahiri, *Dalton Trans.*, 2010, **39**, 8698.
- 82 R. Gheorghe, M. Kalisz, R. Clérac, C. Mathonière, P. Herson, Y. Li, M. Seuleiman, R. Lescouëzec, F. Lloret and M. Julve, *Inorg. Chem.*, 2010, **49**, 11045.
- 83 A. M. P. Peedikakkal and J. J. Vittal, *Chem. – Eur. J.*, 2008, **14**, 5329.
- 84 J. Sun, F. Dai, W. Yuan, W. Bi, X. Zhao, W. Sun and D. Sun, *Angew. Chem., Int. Ed.*, 2011, **50**, 7061.
- 85 M. Nagarathinam, A. Chanthapally, S. H. Lapidus, P. W. Stephens and J. J. Vittal, *Chem. Commun.*, 2012, **48**, 2585.
- 86 V. Safarifard and A. Morsali, *CrystEngComm*, 2012, **14**, 5130.
- 87 V. Safarifard and A. Morsali, *CrystEngComm*, 2011, **13**, 4817.
- 88 L. Hashemi, A. Morsali and O. Buyukgungor, *New J. Chem.*, 2014, **38**, 3187.
- 89 A. Chanthapally, W. T. Oh and J. J. Vittal, *CrystEngComm*, 2013, **15**, 9324.
- 90 H. Ito, M. Muromoto, S. Kurenuma, S. Ishizaka, N. Kitamura, H. Sato and T. Seki, *Nat. Commun.*, 2013, **4**, 2009.
- 91 T. Seki, K. Sakurada and H. Ito, *Angew. Chem., Int. Ed.*, 2013, **52**, 12828.
- 92 G. Liu, J. Liu, Y. Liu and X. Tao, *J. Am. Chem. Soc.*, 2014, **136**, 590.